2008

# Image Processing and Spatial Analysis of Satellite Imagery for Geobiophysical Modeling of Sources for Increased Sediment Yield in the Greenup Pool of the Ohio River

Michael L. Orr

# Image Processing and Spatial Analysis of Satellite Imagery for Geobiophysical Modeling of Sources for Increased Sediment Yield in the Greenup Pool of the Ohio River

Thesis Submitted to

The Graduate College of

Marshall University

In partial fulfillment of

The requirements for the degree of

Master of Science in Physical Science

with an emphasis in Geobiophysical Modeling

By

Michael L. Orr

Committee Members:

Professor James O. Brumfield, Ph.D., Thesis Advisor

Professor Ralph E. Oberly, Ph.D., Graduate Program Coordinator

Professor Anita Walz, Ph.D.

Marshall University

August 2008

## ABSTRACT

### Image Processing and Spatial Analysis of Satellite Imagery for Geobiophysical Modeling of Sources for Increased Sediment Yield in the Greenup Pool of the Ohio River

**By Michael L. Orr**

The study area for this research is the Greenup Pool of the Ohio River, with the Guyandotte River watershed used as a test case. The watershed passes through southwestern West Virginia. The objective of this research was to create and validate a model for extraction of parameters affecting sediment load from satellite imagery and spatial analysis to enrich the data available for the Ohio River. Unsupervised classification, accuracy assessment, map algebra, and suitability modeling were performed to address the research question. In the area selected for this research, extant data consisted of two points approximately 61.8 river miles apart. In many sediment yield models, adequate data is available for velocity, bathymetry, discharge, and sediment load. Results of this research show the potential for remotely sensed imagery and analysis of statistical and spatial relationships in a geobiophysical model to augment investigations of complex systems where conventional data are lacking.



**Keywords:** Ohio River, Geobiophysical Model, Spatial Analysis, Unsupervised Classification, Sedimentation, Erosion, Landsat, Image Processing.

## ACKNOWLEDGEMENTS

I would like to express my gratitude to the following people for their support and guidance during this research. Chandra Inglis-Smith for opening my eyes to the wonderful opportunity that this program offers, and for her support and leadership in the workplace. Dr. James Brumfield, Dr. Ralph Oberly, Juan de Dios Barrios, and Matthew Beckett for introduction and instruction in the intricacies of remote sensing, geobiophysical modeling, and the numerous software packages necessary to meet these ends. Dr. Anita Walz, whose patience and availability for discussion during my days as a neophyte to the concept of digital spatial analysis were greatly appreciated. Dr. Michael Little and Peter Glass for a greater understanding of the interconnectedness of natural systems. Dr. Sanderson and the Huntington District US Army Corps of Engineers for bathymetric data. The College of Science and the Marshall University Graduate College for support of this outstanding program. Michael Anslinger and everyone at Cultural Resource Analysts, Inc. for their understanding and support during this effort. The Nick J. Rahall, II Appalachian Transportation Institute for providing much needed hardware, software, and an understanding and challenging workplace. All of my parents, Mr. and Mrs. Orr, Mr. and Mrs. Danner, and Mr. and Mrs. Slone for their unwavering support. Thanks to my brother, Dr. Randall S. Orr for his support and expertise. Sinaya Dayan for keeping all of these methods fresh in my mind. To my fellow students and friends, thanks for experiencing this with me. Most of all to my beloved wife Susan for her calm guidance and love, without whom none of this would have been possible.

# TABLE OF CONTENTS

# LIST OF FIGURES

# LIST OF TABLES

# CHAPTER I

# Introduction

## *Overview*

The Greenup pool of the Ohio River exhibits significantly elevated sediment loads when compared with neighboring pools. Increased sediment causes problems for floodplains by increasing the frequency and severity of floods, threatens biodiversity through habitat destruction or creation/fostering of adverse conditions, and affects transportation and economic development by affecting the frequency of maintenance dredging and the spoiling of recreational use of the river. Collection of *in situ* data for locating probable sources of increased sedimentation would be cost-prohibitive and time consuming, evidenced by the lack of such data.

## *Geographic Context*

The Ohio River originates where the Monongahela and Allegheny rivers meet in Pittsburgh, Pennsylvania, and empties approximately 981 miles (1579 km) at its confluence with the Mississippi River near Cairo, Illinois (Ohio River Division-USACE 1994). The busiest section of the Ohio River in terms of barge traffic has been the Port of Huntington since it surpassed Pittsburgh in 1953 (Rhodes 2007). Prior to 2000, the Port of Huntington was defined as the 14 mile (22.5 km) section of Ohio River from river miles 303 to 317 (Institute for Water Resources-USACE 2004). In 2000, the Port of Huntington was redefined to encompass 100 Ohio River miles (160.9 km), from river mile 256.8 to 356.8, 90 Kanawha River miles (144.8 km), and 9 miles (14.5 km) into the Big Sandy River, both measured from their confluence with the Ohio upstream (IWR-USACE

2004; Rhodes 2007). The Greenup pool of the Ohio River envelops the former Port of Huntington but is encompassed by the redefined 'Port of Huntington-Tri State' (Figure 1) (Rhodes 2007; IWR-USACE 2004).

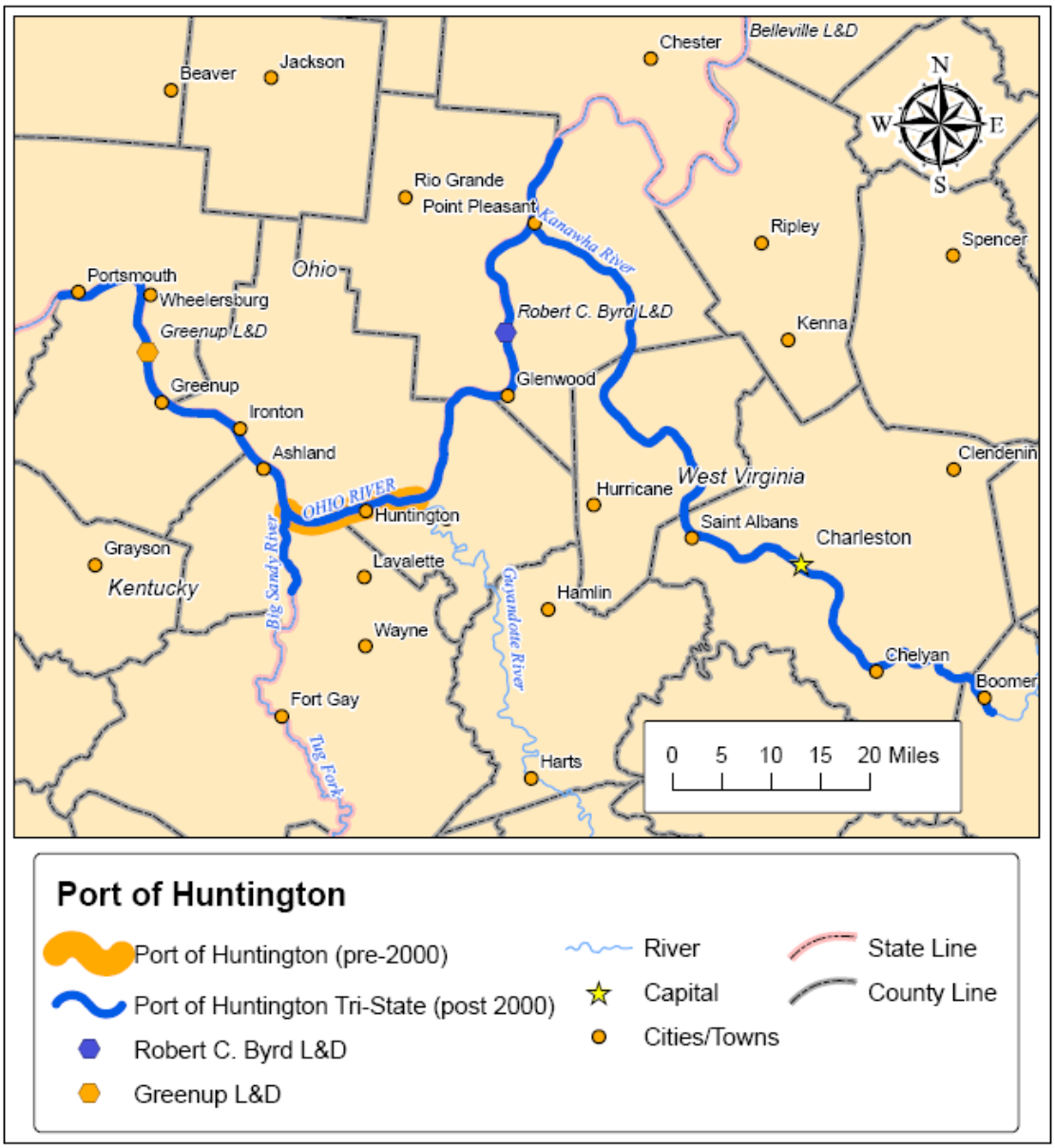


**Figure 1. Port of Huntington Evolution**

The Greenup Pool of the Ohio River flows from the Robert C. Byrd Locks and Dam at river mile 279.2 northwest of Apple Grove, West Virginia, to the Greenup Locks and Dam at river mile 341.0 northeast of Lloyd, Kentucky (Figure

1; Rhodes 2007). The river mile notation used for the Ohio River during this research refers to increasing distance downstream from river origin, which differs from most river mile systems, increasing from the mouth to the head (Ohio River Division-USACE 2006). The Ohio River Basin covers large portions of Pennsylvania, West Virginia, Ohio, Indiana, Illinois, Kentucky, and Tennessee and small portions of Virginia, North Carolina, Maryland, and New York (Figure 2). Within the basin, the Greenup pool is fed by the Middle Ohio and the Big-Sandy-Guyandotte sub-regions, which are further divided into the Guyandotte, Big Sandy, and Middle Ohio-Raccoon basins (Figure 3). Sub-basins are the smallest division used during this research. Divisions for sub-basins are in Figure 3, and Table 1 provides a list of those that empty into the Greenup pool of the Ohio River.

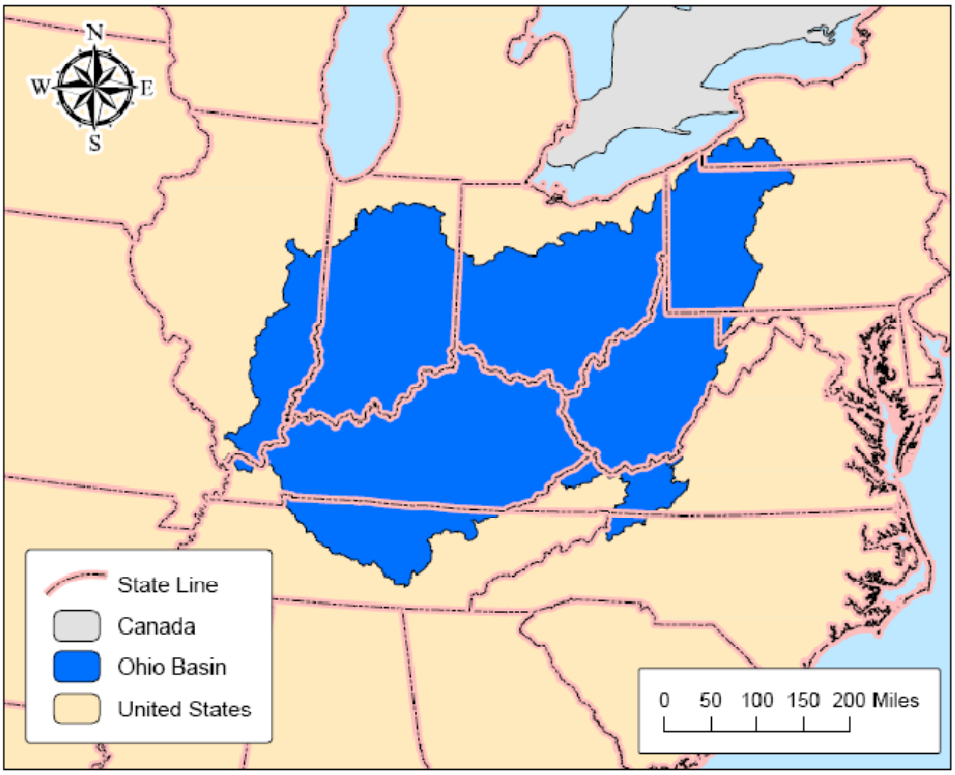


**Figure 2. The Ohio River Basin.**

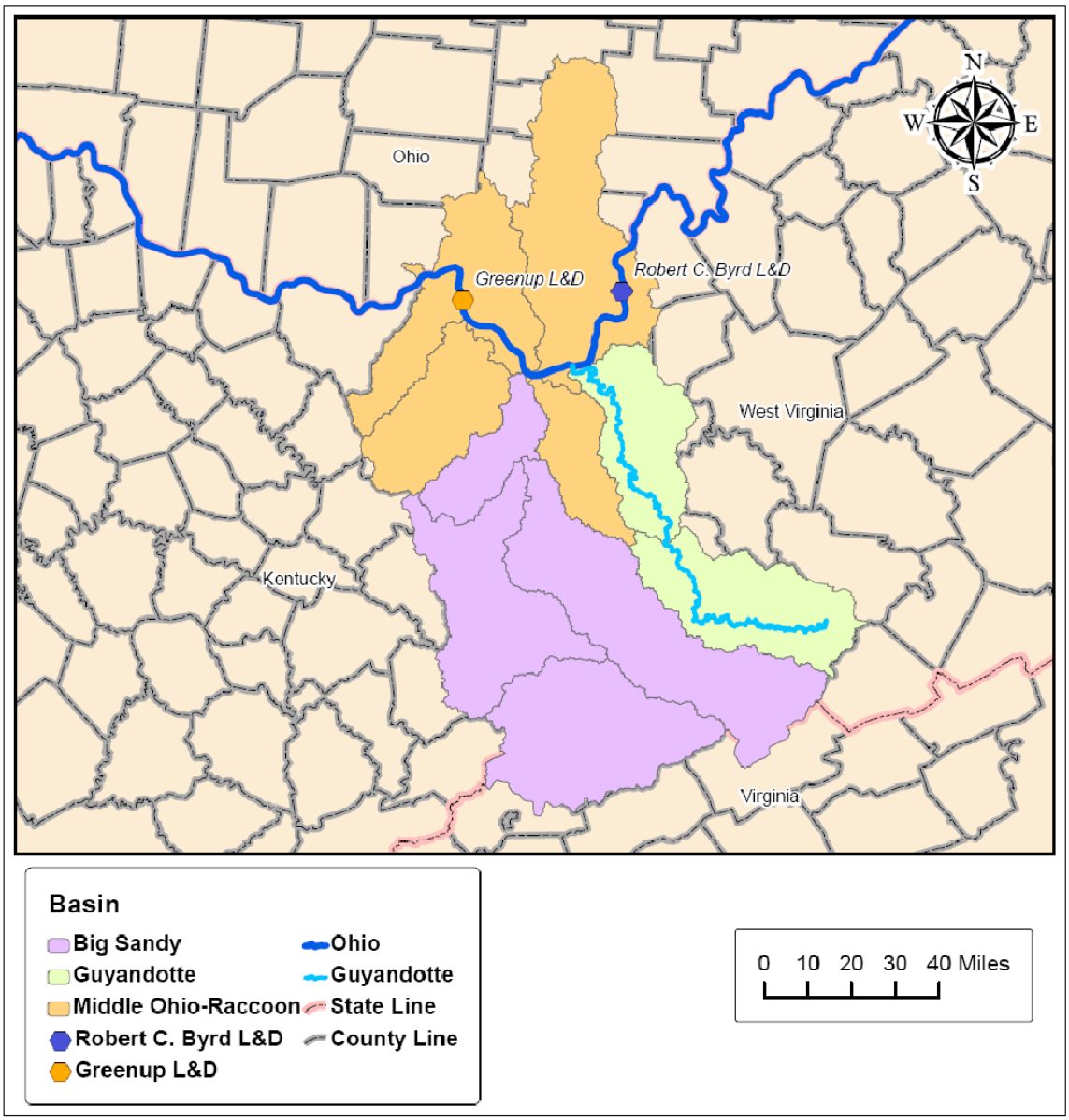


**Figure 3. Basins Feeding the Greenup Pool.**

| Basin | Sub-Basin |
|---|---|
| Big Sandy | Big Sandy |
| Big Sandy | Lower Levisa |
| Big Sandy | Tug |
| Big Sandy | Upper Levisa |
| Guyandotte | Lower Guyandotte |
| Guyandotte | Upper Guyandotte |
| Middle Ohio-Raccoon | Little Sandy |
| Middle Ohio-Raccoon | Little Scioto-Tygarts |
| Middle Ohio-Raccoon | Raccoon-Symmes |
| Middle Ohio-Raccoon | Twelvepole |

**Table 1. Sub-Basins Feeding the Greenup Pool.**

### *Historic Context*

The Ohio River has been a significant transportation route since long before Europeans came to America; however, there was one constant and many seasonal obstructions present that made continuous river commerce between Pittsburgh and the Mississippi River difficult. The falls of the Ohio, a set of rapids near Louisville, Kentucky, that dropped approximately 26 feet (7.9 m) over the course of two miles, were skirted by the 1830 completion of a canal approximately 1.9 miles (3.1 km) long with a navigable depth of 3 feet at low water (Ohio River Division-USACE 1979).

Seasonal variations in river depth made travel of goods unreliable, with evidence of depths of 2 feet (0.6 m) near Huntington recorded in the 1890s (Ohio River Division-USACE 1979). As a result of years of study and the River and Harbor Act of 1910, construction began later that year to canalize the Ohio River from Pittsburgh to the Mississippi to a uniform 9 ft (2.74 m) navigation channel depth. This was accomplished by the construction of 48 navigable wicket dams and two non-navigable dams. The project was finished in 1929 (Ohio River Division-USACE 1979). It is clear from Ohio River Navigation Charts (Figures 4 and 5) that the Ohio had many more exposed sand bars in the early 20$^{th}$ century than are evident today (Ohio River Board of Engineers 1929; Ohio River Division-USACE 2003). Of course, this does not mean that these bars are gone, rather current managed pool height is well above these hazards, as sidescan sonar information provided by the Huntington District of the US Army Corps of Engineers illustrates (Figures 4 and 5). The historic Guyandotte and Twelvepole

bars for example are still present, but are not seen today due to the consistent depth of the river afforded by the lock and dam system. Current sailing lines are nearly identical to the historic charts, and both coincide with the *thalweg*, or greatest channel depth according to 2006 bathymetry (Brewster 2006; Bridge 2003).

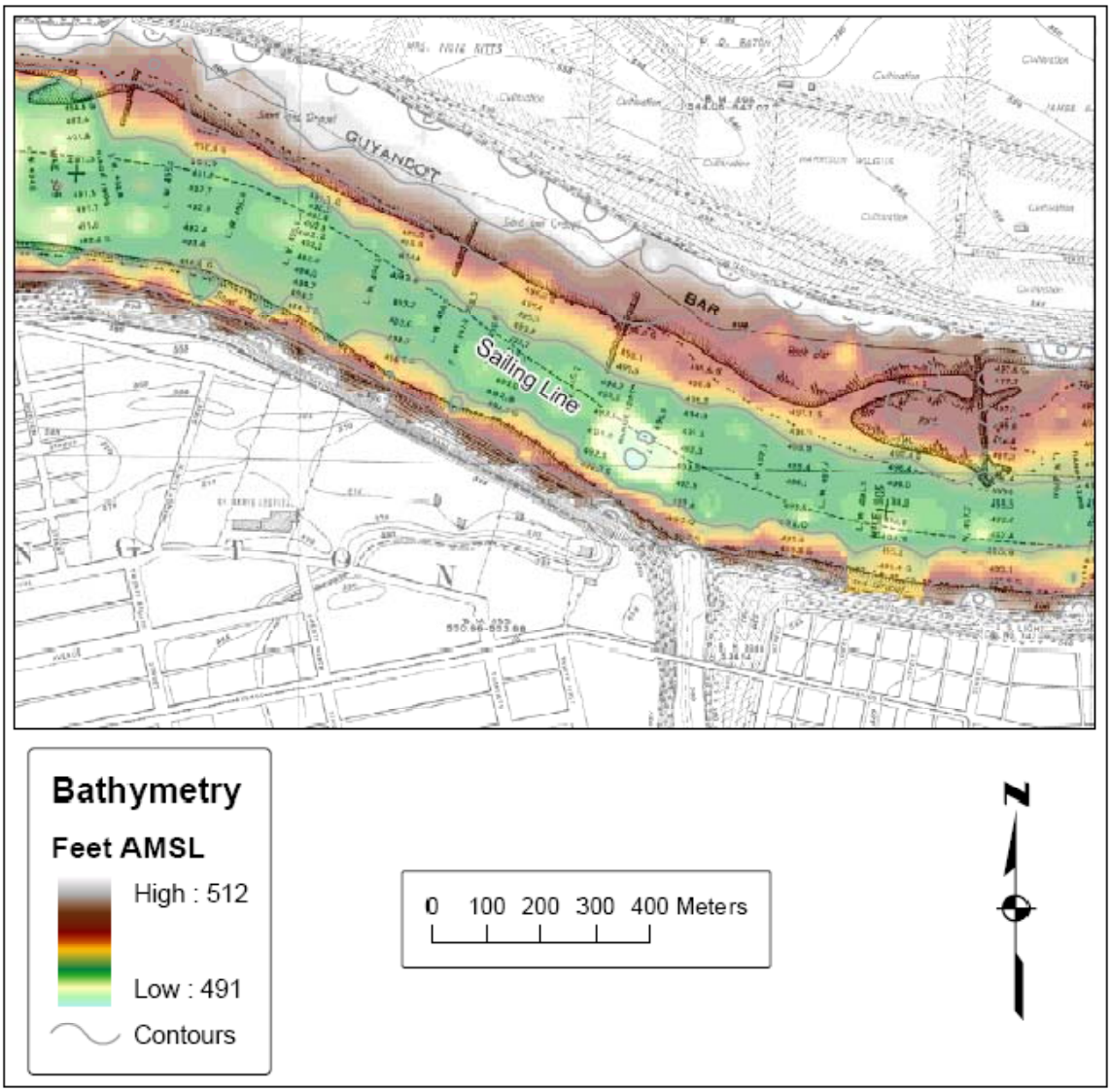


**Figure 4. Navigation Chart No. 84. 1911-1914, revised 1929 over 2006 Bathymetry.**

The Gallipolis Locks and Dam was completed in 1937 and after upgrade in 1992, it was renamed Robert C. Byrd Locks and Dam (Ohio River Division-USACE 1979; Library of Congress 2008). Greenup Locks and Dam marked the beginning of the Modernization Program, which elongated the main lock chamber from 600 to 1200 feet. Construction began in 1954 and the site was operational by 1961 (Ohio River Division-USACE 1979).

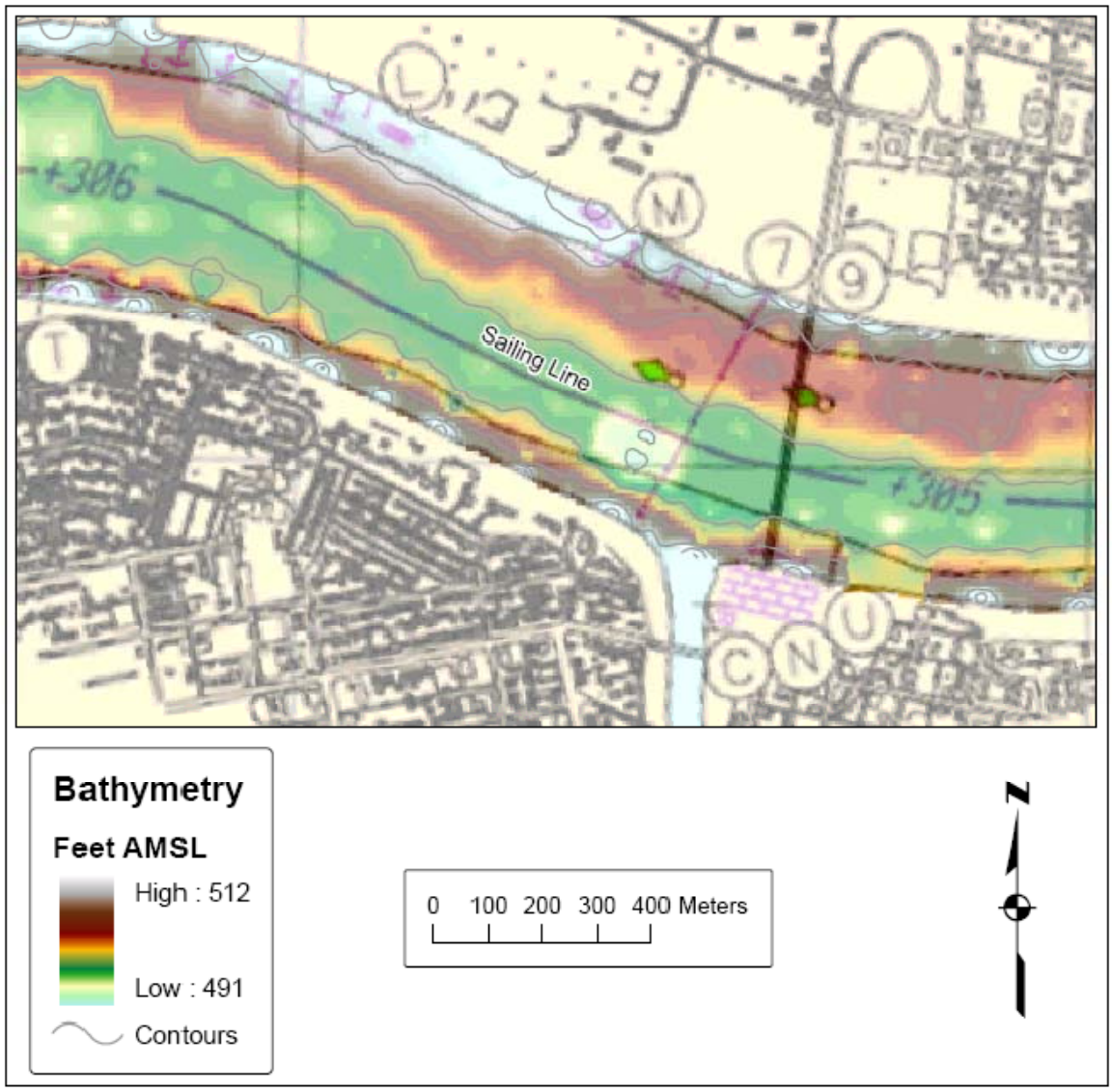


**Figure 5. Chart No. 149, 2003 over 2006 Bathymetry.**

### *Physical Properties*

Within any hydrologic system, transport of solid material is fed primarily by rainfall and groundwater systems, beginning as sheet runoff on steep slopes, and eventually organizes with lessened gradient into streams and rivers (Nichols 1999; Bridge 2003). This is a natural process that occurs anywhere there is precipitation. However, where anthropogenic alterations have occurred, the natural balance is disrupted and detrimental effects can occur (Meijerink & Mannaerts 2000; Bridge 2003; Mather 1986; Easterbrook 1969; Parker 2000; Fitzpatrick, Knox, and Whitman 1999). Affects can range from physical changes in channel structure to alteration or elimination of habitats, with adverse affects on transportation and economic development.

Erosion begins with the products of chemical and physical weathering of parent rock material. The initial step in the erosion process is *entrainment*, or the application of sufficient force to dislodge a particle (Parker 2000). Water is most frequently the source of this initial force, whether as raindrops striking the ground, sheet wash on steep slopes, or flow within an established channel. However, wind, ice, and gravity, or a mixture of all may initiate entrainment as well (Nichols 1999). Among forces that oppose entrainment are electrical and chemical cohesion and vegetation (Parker 2000). Vegetation is so significant a factor that it must be discussed in detail later.

If entrainment is considered an event, then transport is a continual process. Transport continues until the force applied is no longer sufficient to keep the particle moving (Parker 1999). Very fine particles, such as silt and clay, are

often transported in *suspension* or suspended load, where the force of flowing water is sufficient to keep the particle flowing without settling to the bottom (Nichols 2000). Transport of larger particles, such as sand of varying grades, is performed by a series of jumps along the bottom, called *saltation* (Easterbrook 1969). In extreme flows, larger particles may be subjected to this action, such as pebbles and cobbles. More often, these larger particles are moved down stream by rolling along the bottom, a process called *traction* (Easterbrook 1969; Bridge 2003). Both saltation and traction are processes that move the portion of sediments called bed load (Nichols 1999).

Once the process of transportation has ceased, the event of deposition occurs. As mentioned in the preceding paragraph, larger particles require more energy than fine particles to remain suspended or motile, therefore sediments are sorted, with large particles in high energy areas and increasingly finer particles settling as energy decreases (Easterbrook 1969). Common sites for deposition include areas where a significant change in slope occurs, dimensions (width or depth) of channel change abruptly, or there are obstructions such as fallen trees, dams, or other large non-moving objects (Parker 1999). Excessive deposition can create changes in channel structure that encourage increasing rates of deposition.

Catchment land surface vegetation affects the hydrologic system in numerous ways, including impeding runoff, increasing soil porosity, increasing channel friction, and performing evapotranspiration (Leopold, Wolman, and Miller 1964). Vegetation can greatly impede entrainment by sheltering erodible

materials from the full intensity of falling raindrops, and by creating obstacles to sheet wash events (Parker 1999). Another expression of impediment of flow is *surface roughness*. Manning's roughness coefficient, the most commonly used measure of surface roughness, offers values for a wide variety of generalized surface types (McCuen 2005). Historically, transition from natural or minimally affected forested land to row crop agriculture shows a rise in sediment yield, but it is gradual and not extreme in its peaks, whereas abrupt change such as clear-cutting or preparation for urbanization create spikes in sediment yield (Mather 1986; USDA 1996). While clear cutting and construction cause these spikes, if properly managed they can return to near pre-change hydrologic conditions over years or decades, while agriculture tends to be a longer term change that continues its effects (Fitzpatrick et al. 1999). Mitigation procedures for construction or industrial areas include diversion ditches, straw bale sediment barriers, and sediment ponds to decrease velocity and allow sediment to settle.

When trees are removed abruptly by fire or mechanical processes, soil and rock that have been loosened or broken down by roots are suddenly exposed, and highly susceptible to erosion (Mather 1986). However, when the canopy or undergrowth is healthy this loosening of the soil increases permeability, promoting the transformation of surface water into ground water, decreasing erosion (Parker 1999; Leopold et al. 1964). Water percolates easily through zone of aeration made porous by root action, eventually reaching the zone of saturation. The upper limit of this zone is known as the water table. In the eastern U.S., streams are recharged by surface runoff and groundwater, where

the water table intersects valley or stream margins (Easterbrook 1969). Vegetation in a channel, like any other material, increases friction, causing a decrease in stream velocity, which diminishes the erosive power (Easterbrook 1969; Parker 1999). Within a catchment, vegetation also removes water from surface flows and groundwater, known as *interception*, and releases water back into the cycle through *evapotranspiration* (Gorte, 2000).

Within each watershed, there are zones where one of three processes dominate (Figure 6). These processes, which have varied names in the literature, are called *degradation* or vertical downcutting, *transportation*, and *aggradation*, upbuilding, or deposition (Easterbrook 1969). Much of eroded material comes from the upland sections of catchments and stream networks, where the slope is the highest (Fitzpatrick et al. 1999). This coincides with the previous discussion of sheet wash on steep slopes, where vertical downcutting of stream channels has highest influence (Easterbrook 1969). As the slope gradient lessens, the amount of downcutting decreases, and transportation of sediment, mostly in suspension, becomes the dominant process. Addition to the sediment load in this zone is chiefly by lateral erosion of the stream channel (Easterbrook 1969; Fitzpatrick 1999). As the channel continues it reaches a point where the flow does not exert enough force to transport the given load and aggradation or deposition occurs (Easterbrook 1969). This change in flow can be caused by meeting a stream of lower discharge, or by consistent deposits in an area causing the stream to slow down and pool or create large, slowly swirling eddies (Bridge 2003). While this model is descriptive of the entire span of a stream,

these processes also occur to some degree in very short spatial and temporal spans, yielding the widespread morphologic variation of a stream channel.

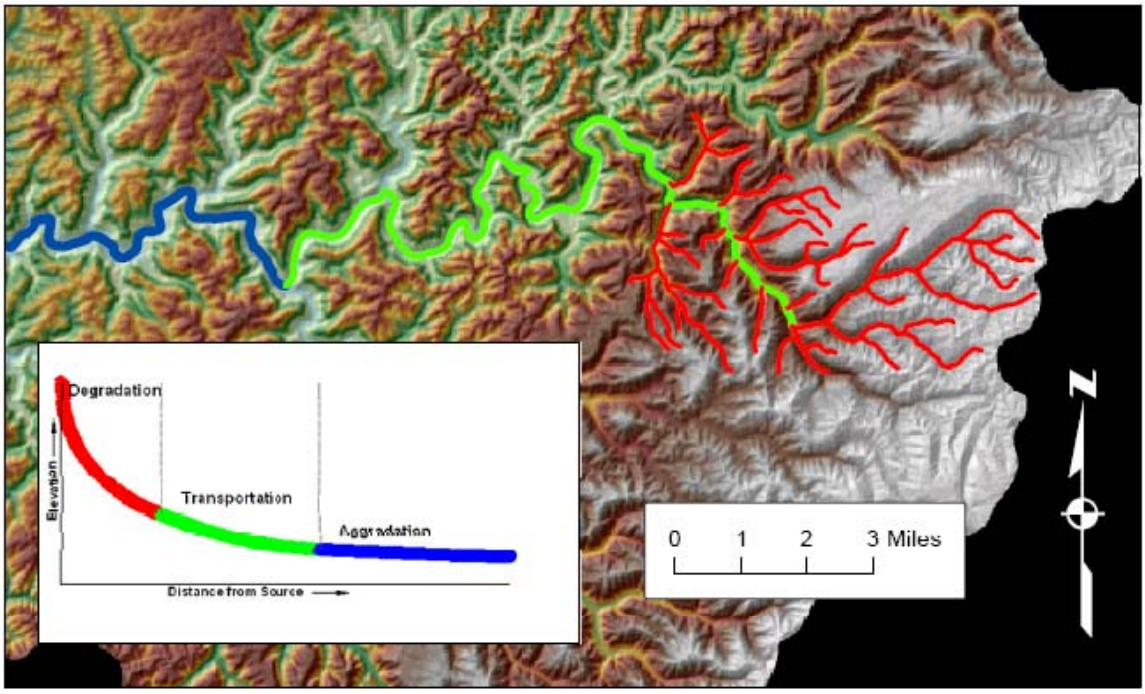


**Figure 6. Dominant Zones of Degradation, Transportation and Aggradation.**

Within an idealized channel, velocity is highest in the middle, slightly below the surface (Figure 7). Friction from the banks decreases velocity in plan view, while in profile, friction from the bed or bottom affects velocity more than friction caused by the air-water interface (Easterbrook 1969; Bridge 2003). Given this empirical plan and cross-section, vegetation's role, scouring and shifting of bed load, and large debris in the bed and along the bank walls, it is clear that velocity in an actual channel will have wide variation. The highest velocity vector will be very different from the velocity of the sides and bed. Bridge piers and

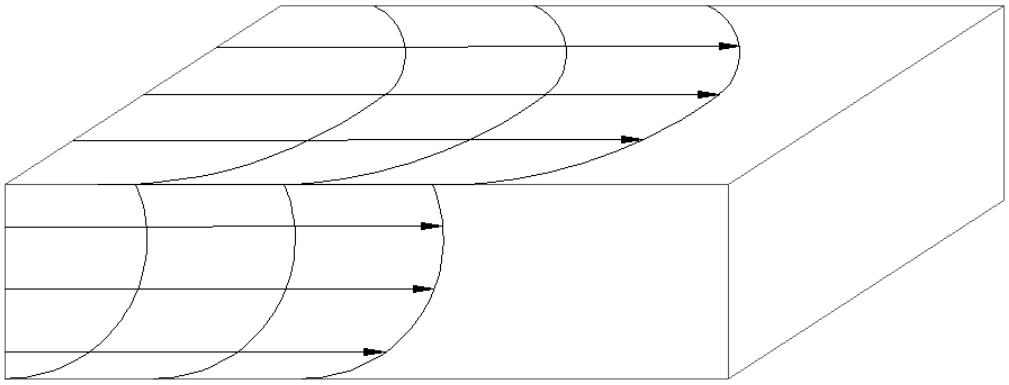

**Figure 7. Velocity Vectors in an Idealized channel (adapted from Easterbrook 1969).**

other manmade obstructions can further impede flow, however uniform and symmetrical obstructions such as bridge piers may create a *Karman vortex street*, which sheds vortices of opposite rotation from either side of the object and can run vertically from the surface to the bed, churning substrate throughout the water column (Bridge 2003). During floods, the highest velocity again tends to be in the center of the channel, while the quickest lateral decrease of velocity is at the bank interface, and velocity of flow over the flood plain is considerably less than the center of the channel (Bridge 2003). The relationship between stream velocity and particle size and its relation to the previous discussion of erosion, transportation and deposition is summarized in Figure 8, (adapted from Easterbrook 1969; Parker 2000).

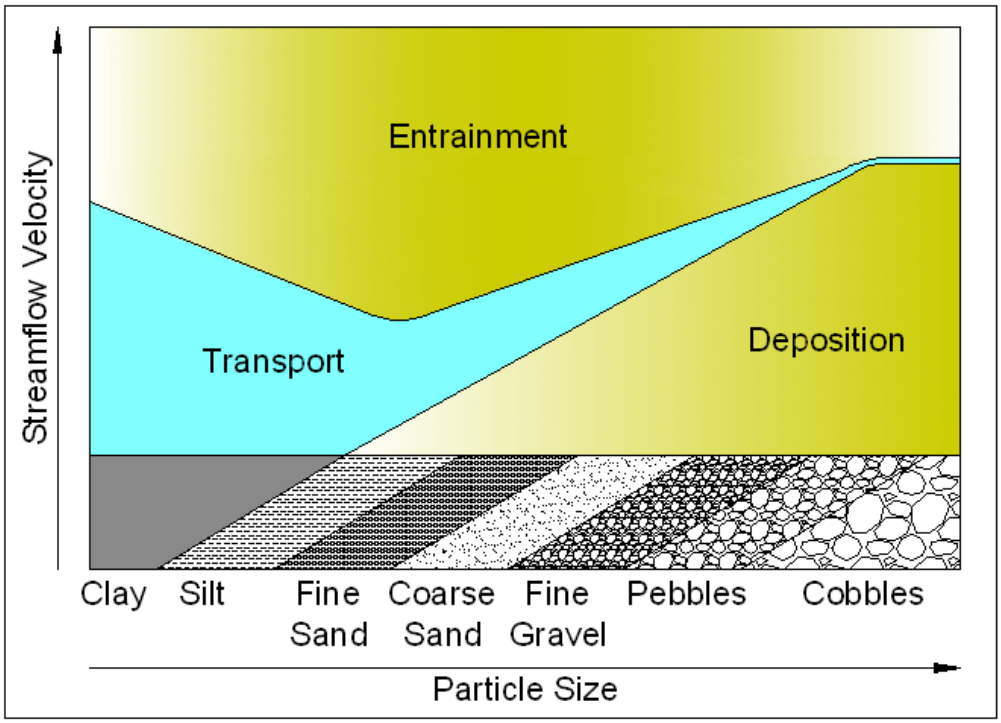


**Figure 8. Relations among Erosion, Velocity, and Particle Size (adapted from Parker 2000).**

### *Biological Affects*

The affects of sedimentation on biota include habitat loss due to changes in channel structure, alteration of stream temperature and composition, and impediment of light penetration through the water column (Ellis 1936; Cushing and Allan 2001). Loss of habitat for individual species has a direct effect on the food web, which can decrease biodiversity in a given area.

Excessive erosion can deposit particulate matter that is finer than the dominant macroinvertebrate community can tolerate. For Example, many species prefer or thrive in areas with bed materials of cobbles or pebbles, therefore deposition of finer particles such as silts and sands can have direct affects to the local food web (Cushing and Allan 2001). As previously stated, this deposition

can occur due to increased load from anthropogenic sources or from decreased velocity from prior deposition or other obstruction. While all substrate materials can support algae, stable surfaces tend to produce larger communities, increasing surface roughness and heterogeneity, which is conducive to greater biodiversity (Cushing and Allan 2001).

Increased siltation can directly affect the temperature of streams, as has been shown in experiments using both agitated and unagitated water containing sediment (Ellis 1936). Ellis' experiment showed that in agitated water, there was no marked difference between the control (distilled water) and unfiltered field samples when immersed in a bath of a constant temperature. There was a significant lag (17 minutes) in temperature change over time in the unagitated unfiltered water compared to the control, with differences as great as 1.8°C (3.2°F), while there was only as great as a 0.1°C (0.2°F) difference between an unagitated filtered sample and the control. Indirectly, deposition can affect water temperature by destruction of riparian vegetation, exposing water to direct sunlight (Cushing and Allan 2001).

Increased sediment can also be implicit in destruction of macroinvertebrate and algal communities by insufficient oxygen levels to the organism or starvation (Ellis 1936; Cushing and Allan 2001). In another experiment by Ellis, fresh-water mussels were observed in water containing suspended silt and water that was silt free. Mussels in the silty water remained shut (not feeding) 75-95% of the observed time, and when they did open, excessive mucus was secreted to remove silt from the mantle cavity. Members of

this group that did not survive contained deposits of silt in the mantle cavity and gill chambers. Members of the silt free group were closed less than 50% of the observed time (Ellis 1936).

Turbidity, or the opacity of water, caused in part by increased sediment load, can be measured in the field by *Secchi disk* or in samples by *nephometric turbidity units* (NTU) (Campbell 2002). Ellis measured turbidity using a scale called the *millionth intensity depth* (m.i.d.), which is the depth at which light is reduced to one millionth of its surface intensity, measured in millimeters. Regardless of the unit or method of measure, the effect on plants is simple: where there is consistently little to no light penetration, there will be little or no material dependent on photosynthesis. There was a bias toward penetration of the scarlet-orange wavelengths (λ = 0.660 – 0.585 μm) in the turbid water of 88 mm m.i.d. (Ellis 1936). This differs from clear water, wherein red light is absorbed in the first 2.0 m (6.6 ft) and blue-green wavelengths (λ = 0.48 to 0.60 μm) can penetrate beyond 100.0 m (328.1 ft). Blue light (λ = 0.40 to 0.50 μm) can penetrate water beyond 275.0 m (902.2 ft), but is highly susceptible to scattering (Campbell 2002; NASA 2008). Transmission of any light was minimal, and the overall effect of increased turbidity was a nearly complete blockage of all visible wavelength penetration (Ellis 1936).

### *Anthropogenic Affects*

The largest role of transportation, industry, and economic development in increased sedimentation can be stated simply: an increase in impervious surfaces (roads, parking lots, roofs, etc.) means an increase in surface runoff

with very little friction, meaning a higher sheet wash velocity (Mather 1986; Fitzpatrick et al. 1999). An increase in the volume and velocity of surface runoff brings an increase in debris and sediment transport, and a decrease in ground water infiltration. A decrease in infiltration means that the soil is drier and less cohesive, thus more susceptible to sheet erosion (Scheyer and Hipple 2005). This decrease would also lower the rate of groundwater recharge of streams, making them more susceptible to wider fluctuation in flow, chiefly dependent on rain events (Easterbrook 1969). Due to the efficiency of drainage systems in urban settings, flood peaks are frequently increased by a factor of three or four when compared to the countryside, generating even more erosive power (Mather 1986).

The construction phase of these impervious surfaces, while temporary, can also be a significant source of sedimentation, estimated anywhere from 2 to 40,000 times the preconstruction sediment delivery rate (McCuen 2005; USDA NRCS Soil Quality Institute 2000). Exposure of bare earth to erosive forces is more long term and widespread in industrial activities such as logging and mining, thus offering significant sources of sediment (Mather 1986; McCuen 2005; Scheyer and Hipple 2005; Cushing and Allan 2001; Leopold et al. 1964).

Dredging for channel depth maintenance is required annually and supplemented on an as-needed basis. In the Greenup pool, channel maintenance dredging occurs annually in late summer during periods of low water, usually mid-August. Dredging does not occur uniformly throughout the pool each year. For example, the mouth of the Guyandotte River area has not

been dredged since 2000. The area around the Robert C. Byrd locks and dam is dredged more frequently, as is the Big Sandy River (USACE Staff, personal communication 2008).

This action has a direct effect on habitats either by physical removal, or by increased turbidity and reintroduction of settled materials into suspension (USACE 2006). Deposition occurs often at the interface of streams and where water is abruptly slowed, such as dams, thus in order to maintain the channels, regular dredging must be performed. As an example, excessive sedimentation makes the Big Sandy River impassible beyond approximately 7.5 miles. Dredging could be performed beyond this point, however the availability of other modes of transportation running from the major resources skew the cost-benefit analysis toward existing infrastructure, having a direct effect on location of intermodal facilities (ORD-USACE 1994). For an example of the impact on economic development, the Corps of Engineers found, based on user interviews, that local marinas found it too expensive to maintain embayments by way of systematic dredging, limiting public use of sections of the river (ORD-USACE 1994).

Coal extraction is the largest industry on the Ohio River as expressed in tonnage of commodity shipped, and the most productive areas in the nation are centered on the Kanawha and Big Sandy rivers, making transport through at least some portion of the Greenup pool very likely (ORD-USACE 1994; 2006). In 2003, coal and coke accounted for 118.5 million tons of commodities shipped on

the Ohio River. The next highest tonnage was aggregates (sand, gravel, limestone, etc.), followed by petroleum (Table 2; USACE 2006).

| Commodity | Million Tons |
|---|---|
| Coal & Coke | 118.5 |
| Petroleum | 16.3 |
| Aggregates | 41.7 |
| Grains | 13.8 |
| Chemicals | 10.3 |
| Ores & Minerals | 7.4 |
| Iron & Steel | 13.9 |
| Other | 6.8 |
| **Total** | **228.7** |

**Table 2. Commodity Traffic on the Ohio River, 2003.**

The coal industry is affected by increased sedimentation in the form of increased shipping costs to offset dredging operations, time lost by interference from dredging operation, and point bar hazards to barges. It is also a major cause of increased sedimentation, due to deforestation and bare earth for extended periods of time (McCuen 2005; Mather 1986; Cushing and Allan 2001; Leopold et al. 1964; Scheyer and Hipple 2005). Logging, which tends to preclude most mining activity, has a similar affect on hydrology, but it also adds very sinuous and poorly kept roads that act as conduits of sediment directly into streams from ridgetops and sideslopes (Cushing and Allan 2001; Orr 2005).

Shipping on the Ohio River is carried out predominantly by a system of barges and tows, although some container ships are used as well. By comparison, one barge can carry the equivalent of 15 jumbo hopper cars (1500 tons), or 58 large semi trucks. One tow can move 15 barges (22,500 tons), equivalent to 225 jumbo hoppers or 870 semi trucks for roughly the same amount of energy (ORD-USACE 1994; 2006). The current average output of these tow/push vessels within the Ohio River Main Stem is 3500 HP, while those on

tributaries tend to be lower (USACE 2006). The action of these engines and displacement of these trains of vessels (15 barges and a tow/push vessel) cause agitation of bed load and substrate along banks due to wake action. The depth of water needed to float a ship, or *draft*, for vessels in the Port of Huntington - Tristate ranges from 1 to 11 feet (0.3 – 3.4 m) (IWR-USACE 2004). The minimum depth of the navigation channel is 9 feet (2.7 m), therefore, the largest vessels can only operate in certain sections of the channel or seasonally, during high water conditions. Temporal data involving when deep draft (draft > 9 ft) can navigate the Greenup Pool are currently lacking. Decreasing cargo decreases the draft of the vessel, thus in certain low water conditions, tonnage is restricted. Temporal variations in lockage through the Greenup locks and dam suggest that March has the highest monthly average traffic, Thursdays and Saturdays are favored weekly, and approximately 10 P.M. sees the highest traffic daily (USACE 2006). These variations are slight and are not considered likely to produce significant difference in sedimentation rates.

### *Statement of Problem and Proposed Solution*

Ohio River Valley Water Sanitation Commission (ORSANCO) collected data from July, 2001 to May, 2005 at several points along the Ohio River. Data from the Robert C. Byrd and Greenup Locks and Dams show marked differences between the two locations in the amount of suspended solids, especially during seasonal runoff periods (Figures 9 and 10). While this shows that there is a phenomenon occurring between the two lock and dam structures that are approximately 61.8 river miles apart, it would be more useful to pinpoint from

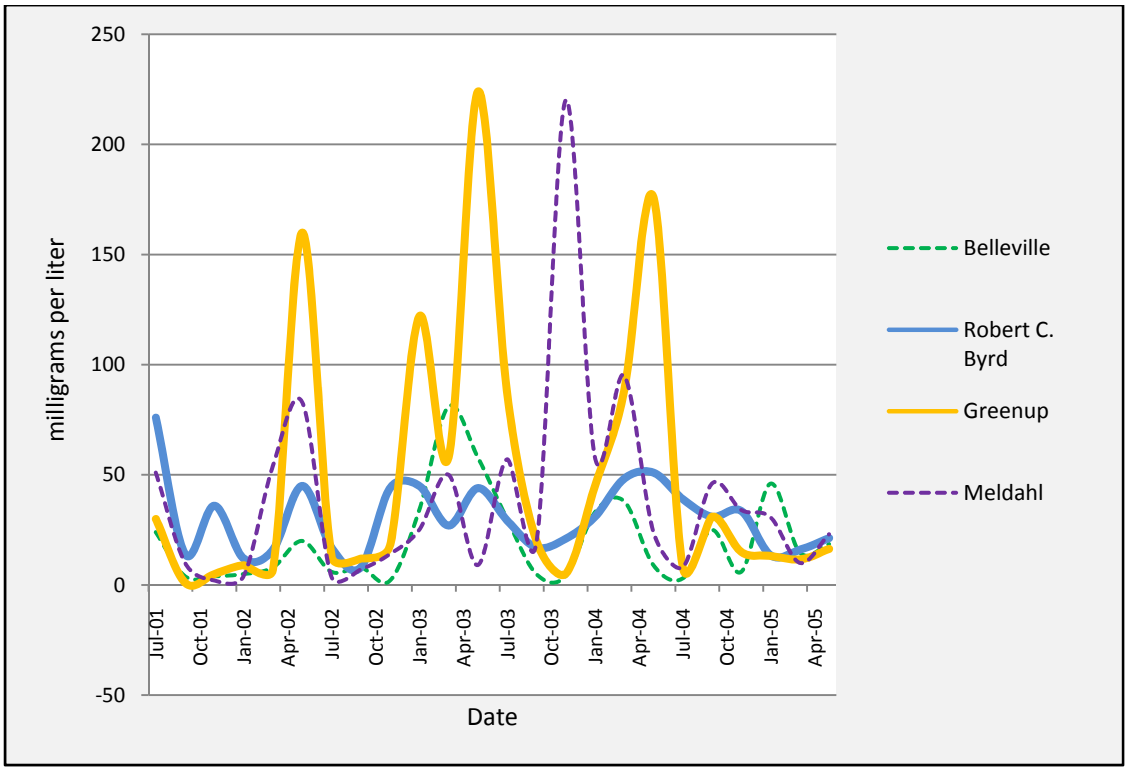


**Figure 9. Bi-monthly Suspended Solids (mg/L) from ORSANCO 7/2001 to 5/2005.**

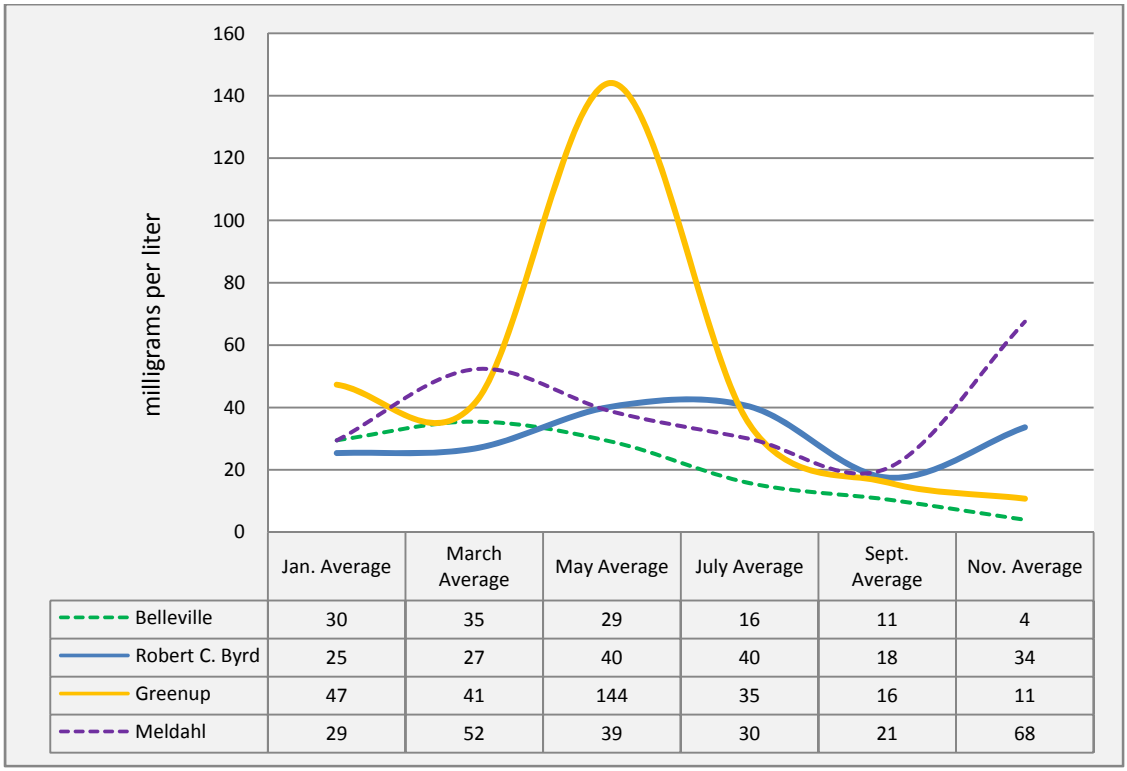


| | Jan. Average | March Average | May Average | July Average | Sept. Average | Nov. Average |
|---|---|---|---|---|---|---|
| Belleville | 30 | 35 | 29 | 16 | 11 | 4 |
| Robert C. Byrd | 25 | 27 | 40 | 40 | 18 | 34 |
| Greenup | 47 | 41 | 144 | 35 | 16 | 11 |
| Meldahl | 29 | 52 | 39 | 30 | 21 | 68 |

**Figure 10. Monthly Averages of Suspended Solids (mg/L) from ORSANCO 7/2001 to 5/2005.**

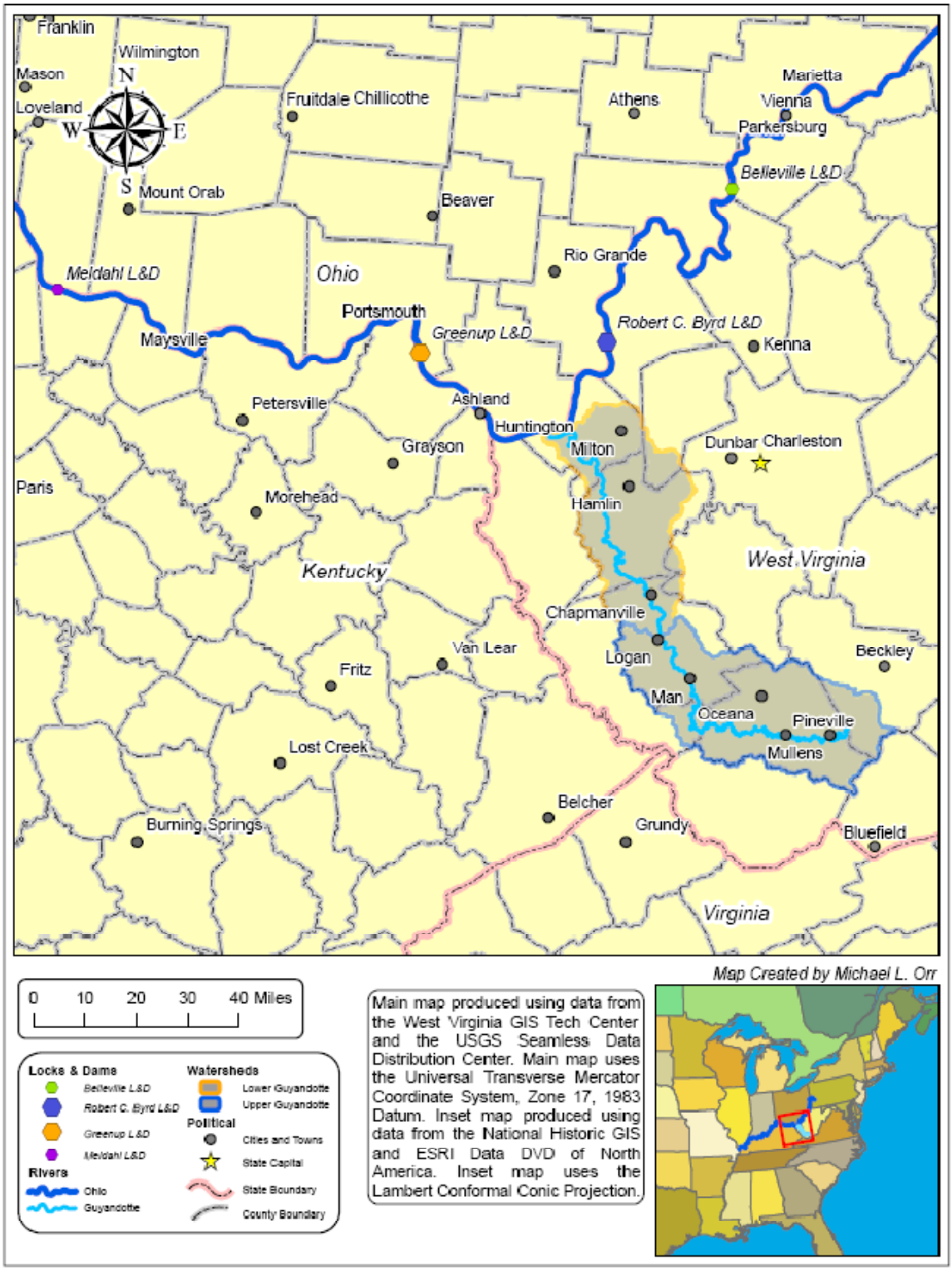


**Figure 11. Extent of Guyandotte Watershed, Ohio River, and Bounding Locks and Dams.**

whence these sediments came. As previously mentioned, sediment load data sufficient to address this problem is scarce, costly, and time consuming to collect. Therefore it is the objective of this research to use satellite imagery, image processing, and spatial analysis to create and validate a model to show sources for increased sediment yield. This pilot study will assess techniques that can be used in future research to further address causes for the discrepancy between Robert C. Byrd and Greenup collection points (Figure 11).

# CHAPTER II

## Research Methods and Techniques

### *Overview*

The Guyandotte River watershed passes through southwestern West Virginia in a southeast to northwest direction, touching Boone, Cabell, Kanawha, Lincoln, Logan, Mingo, Putnam, and Raleigh counties, and encompassing Wyoming County (Figure 11). Area of the watershed is 1,076,930 acres (435,818 ha), or 1,683 square miles (4,358 sq km). It is located in the maturely dissected upland of the Appalachian Plateau. Elevation ranges from 3581 ft (1091 m) above mean sea level (AMSL) in Wyoming County to 512 ft (156 m) AMSL at the confluence of the Guyandotte and Ohio rivers (Figure 12; Wolf 1988). Bedrock Geology belongs to the Pennsylvanian period. More specifically, Guyandotte River flows through Pottsville group New River formation to Kanawha formation, through the Conemaugh group and Allegheny formation and meets the Ohio River in Quaternary Alluvium (Figure 13). Soils are generally deep, well drained, and on steep sideslopes to nearly level floodplains having weathered from sandstone with some shale and siltstone present (Cole 1989; Cole, Carpenter, and Delp 1985; Gorman and Espy 1975; Jones 2007; Van Houten, Childs, Teets, Estepp, and Doonan 1981; Wolf 1988 and 1994). Major tributaries of the Guyandotte River include Big Ugly, Buffalo, Huff, Indian, Island, and Pinnacle creeks, Clear, Slab, and Trace forks, Winding Gulf, and Mud River.

Towns within the watershed include Pineville, Mullens, Oceana, Man, Logan, Chapmanville, Hamlin, Milton, and Barboursville, among others. Transportation in the watershed consists of roads, rail, and airfields (Figure 14).

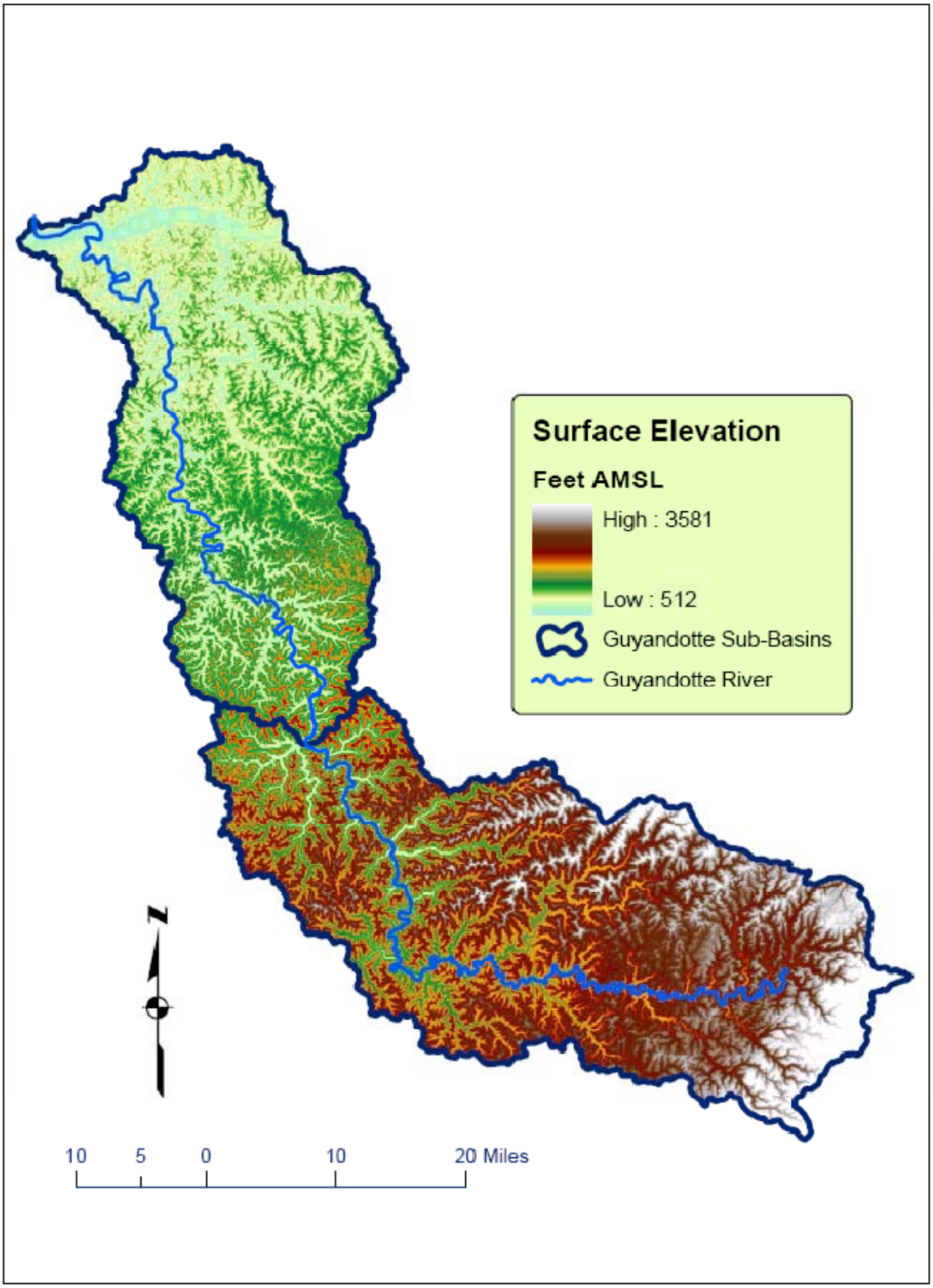


**Figure 12. Elevation within the Watershed.**

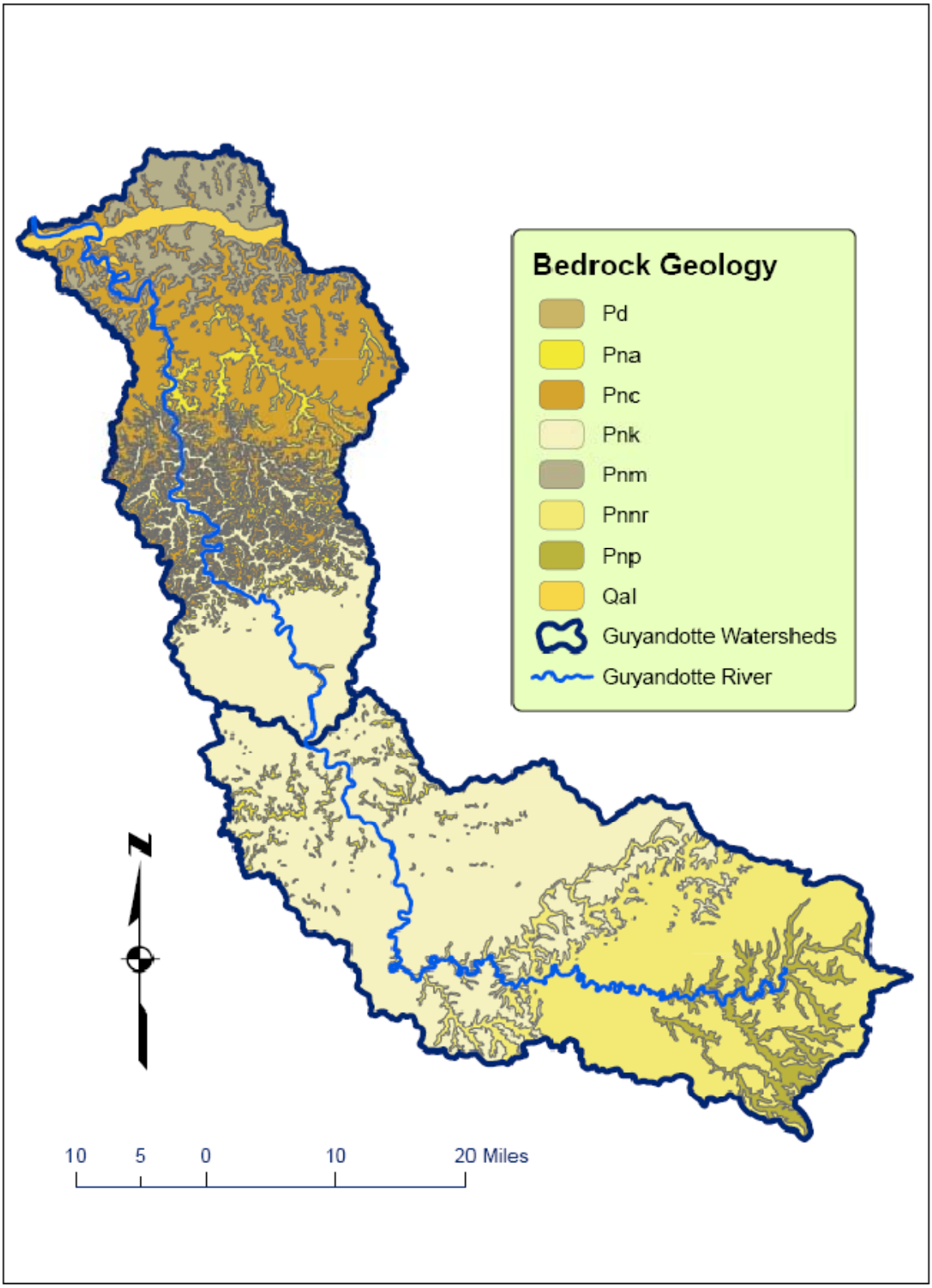


**Figure 13. Bedrock Geology within the Watershed.**

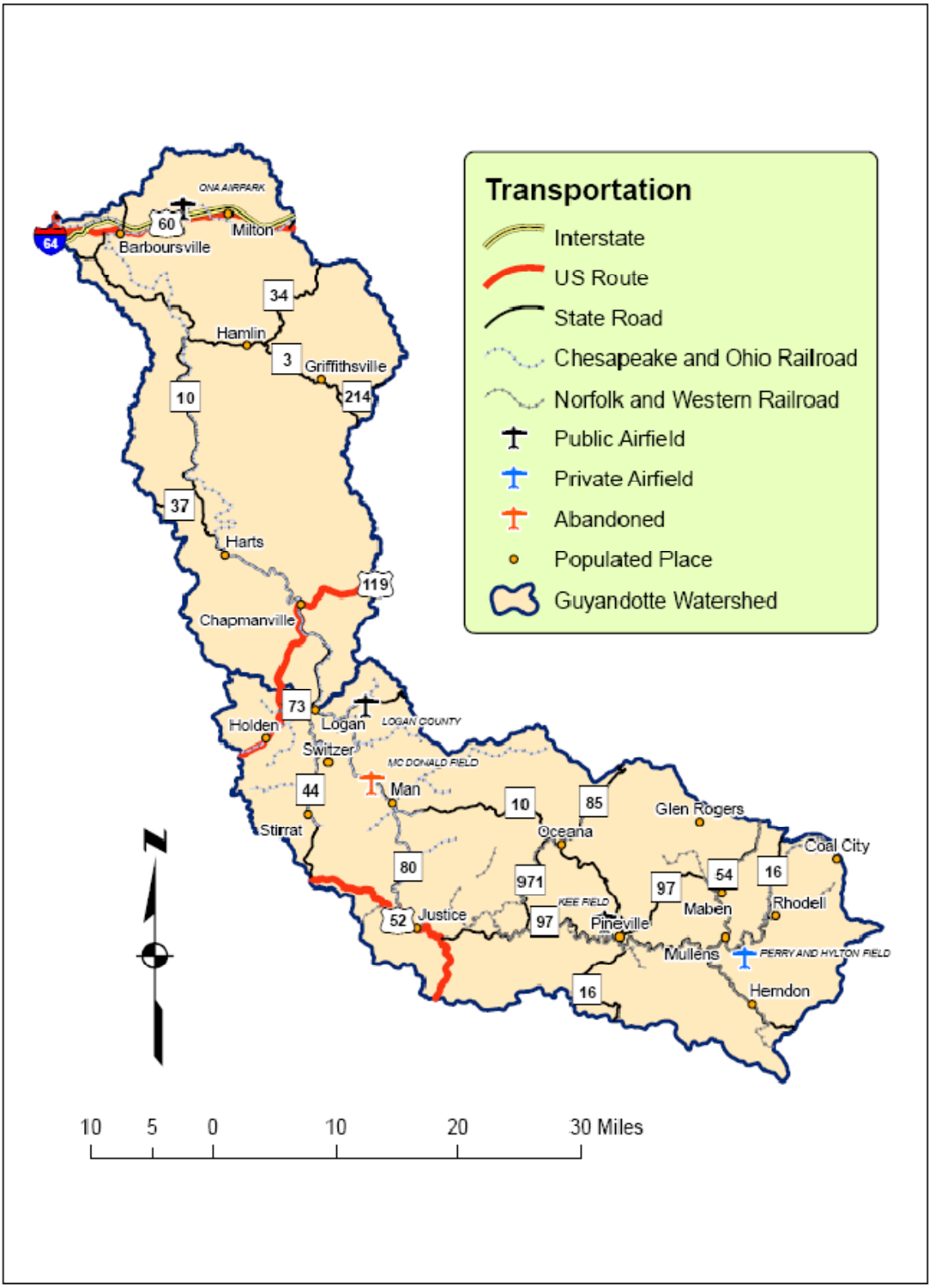


**Figure 14. Transportation within the Watershed.**

State route 10 runs through the center of the watershed, providing access from Herndon to Barboursville and I-64. US routes 119 and 52 cross the watershed briefly in the central and southern portions. Additional access is provided by state and county routes. Railroads offer freight transport from the coal fields north toward Huntington and the Ohio River. The two main lines are the Chesapeake and Ohio and the Norfolk and Western railroads. Of the five airfields in the watershed, three are public access, one (McDonald Field) is abandoned, and one (Perry and Hylton, or Mike Ferrell Field) is private.

### *Remote Sensing Methods*

Remote Sensing is defined, almost universally, as the collection of data about an object or area by sensors that are not in direct contact with the target (Lillesand and Kiefer 1987; Jensen 2000, 2005; Sabins 2007; Aronoff 2005; Wilkie and Finn 1996; Campbell 2002; Schultz and Engman (eds.) 2000; Purkis 2004; Lo 1986; Lintz, Jr. and Simonett (eds.) 1976; Rees 1990). While the current definition is focused strongly on electromagnetic radiation and its interaction with the target, SONAR (sound navigation and ranging) is variably included or excluded from the definition (Sabins 2007; Rees 1990).

The electromagnetic spectrum is a key principle in remote sensing systems. As seen in Figure 15, Energy ranges from the high frequency ($\nu$), short wavelength ($\lambda$) gamma rays ($\lambda < 10$ pm) to the low frequency, long wavelength radio waves ($\lambda > 10$ cm) (Sabins 2007). Radiation used most frequently by current sensors is clustered in the visible to thermal infrared regions ($\lambda = 0.4$ to ~15 μm) and portions of the microwave region ($\lambda = 2.5$ cm to ~30cm) due to

atmospheric absorption and scattering, also referred to as *attenuation* (Rees 1990; Campbell 2002; Jensen 2005; Lo 1986).

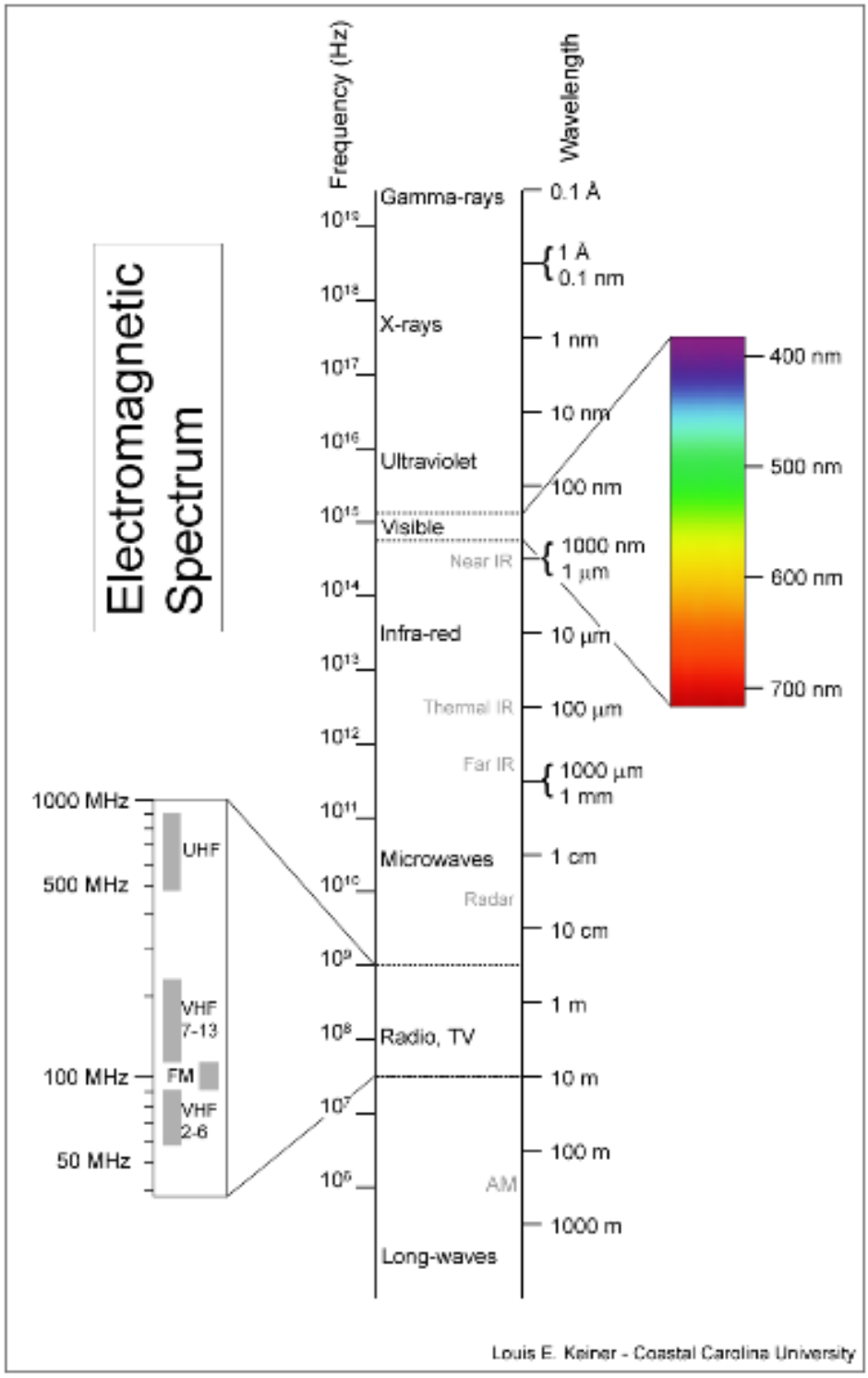


**Figure 15. Electromagnetic Spectrum (Wikipedia.org 2008).**

In passive remote sensing systems, the sensor collects reflected radiation (wavelength, or $\lambda < 3\mu m$), usually generated by the sun, or emitted ($\lambda > 3\mu m$) radiation from an object. These include satellite imagery, aerial visible and false-color infrared photography, and thermal scanners, among others (Campbell 2002; Rott 2000; Aronoff 2005; Sabins 2007; Jensen 2000, 2005). Active systems, or systems that generate electromagnetic or sonic energy that hits the target and is measured as it returns to the sensor, include RADAR, LiDAR, and SONAR (Campbell 2002; Rott 2000; Aronoff 2005; Sabins 2007; Jensen 2000, 2005).

When these returns, or brightness values, are collected digitally, as is most frequently the case, each is assigned to a pixel with a unique column and row address (Tomlin 1990; Aronoff 2005). The area of ground represented by each pixel is equal to the instantaneous field of view and *spatial resolution* attainable by that specific sensor. In order for a sensor to be able to resolve a specific object or phenomenon, the feature's minimum dimension should be equal to or greater than the width of two pixels (Aronoff 2005; Jensen 2005; Sabins 2007). An example of low spatial resolution is the Geostationary Operational Environmental Satellite (GOES) system, with 1 km pixels in the visible spectrum, and 4 to 8 km pixels in the thermal infrared regions (Aronoff 2005). Medium resolution is exemplified by the Landsat Thematic Mapper (TM) with 30 m pixels in the visible to near and short wave infrared bands and 90 m pixels in the thermal band (Sabins 2007; Jensen 2005). Another example of

medium spatial resolution comes from the Advanced Spaceborne Thermal Emission and Reflection Radiometer (ASTER) aboard NASA's Terra satellite, with 15 m visible to near infrared bands, 30 m short wave infrared bands, and 90 m thermal infrared bands (Aronoff 2005; Jensen 2005). High spatial resolution is shown by the Quickbird Satellite from Digital Globe, with 2.44 m pixels in the blue through near infrared bands, and 0.61 m in the panchromatic band (Aronoff 2005; Jensen 2005).

In addition to spatial resolution, there are three other qualities that can be used to assess the specific utility of a particular collection of imagery or information: spectral, radiometric, temporal resolution. *Spectral resolution* is defined as the number and width of bands recorded within imagery (Aronoff 2005; Inglis-Smith 2006). An example of a multispectral sensor comes from ASTER: there are 14 bands, and bandwidth for the near infrared band is 0.1 μm, ranging from 0.76 to 0.86 μm (Aronoff 2005). An example of a hyperspectral system is the Airborne Visible/Infrared Imaging Spectrometer AVIRIS), with 224 10 nm bandwidth bands ranging from 0.4 to 2.5 μm (Sabins 2007). *Radiometric resolution* refers to the ability of a sensor to discriminate between different signal levels of returned radiation (Aronoff 2005; Wilkie and Finn 1996). Landsat TM records information in values from 0 to 255 (8-bit), while Quickbird collects in 11-bits, or values from 0 to 2047, exhibiting higher radiometric resolution (Jensen 2005). Finally, *temporal resolution* is the measure of return time, or the frequency of data collection for the same geographic entity. Examples include Landsat 4, 5, and 7, with a return time of 16 days, and Advanced Very High Resolution

Radiometer (AVHRR), with a return time of 12 hours. AVHRR has higher temporal resolution than the Landsat group (Aronoff 2005).

Land use and land cover are often thought of synonymously, however there are distinct differences (Rees 1990, Anderson, Hardy, Roach, and Witmer 1976; Lillesand and Kiefer 1987). Land use refers to human utilization of the land and its resources, for example, mining, timbering, agriculture, and recreation (Jensen 2000; Inglis-Smith 2006). Land cover refers to the geobiophysical conditions on the ground surface, for example: stands of deciduous trees, open land, urban impervious land, residential grasses, etc. (Lillesand and Kiefer 1987; Aplin 2004). The classification system developed for the USGS in 1976 was a hybrid of the two ideas, which is no doubt a primary reason for the casual intermingling of the terms (Anderson et al. 1976; Lillesand and Kiefer 1987).

The National Land Cover Dataset (NLCD) was first created in 1992, consisting of a 21-group classification system of land cover for the conterminous United States (Vogelman, Sohl, Campbell, and Shaw 1998; Homer, Huang, Yang, Wylie, and Coan 2004). Subsequent changes have been made, including NLCD 2001 and an update for 2006 that is unfinished at the time of this research (Homer, Dewitz, Fry, Coan, Hossain, Larson, Herold, McKerrow, VanDriel, and Wickham 2007; USEPA-MRLC 2007; Vogelman et al. 1998). The highest frequency of land cover classes in West Virginia are deciduous forest (76%), pasture/hay (8%), low intensity residential (5%), and evergreen forest (3%) (Homer et al. 2007; West Virginia University GIS Technical Center 2007).

Remote sensing of various parameters of hydrology and water quality is a difficult, time consuming and costly process. Water quality can be assessed, but due to the ephemeral nature of water data and the dynamic nature of hydrologic systems, imagery collected two weeks ago cannot provide information necessarily relevant today, whereas terrestrial studies can have more flexibility in collection times. Therefore, any *in situ* data (water samples using Secchi disk or NTUs) should be from the same day as any imagery if possible (Jensen 2000). Assuming that these criteria are met, in order to make any statements that have relevance to more than just a single day or even hour, many of these paired datasets must be collected to examine trends and utilize time, or the fourth dimension (Schultz and Engman 2000). Recent research has assessed an alternative method of using ground penetrating radar to collect discharge and velocity measurements without having instruments in the water, however the method still requires very expensive equipment (Haeni, Buursink, Costa, Melcher, Cheng, and Plant 2000). Other current research exhibits promising applications of wide-swath radar altimetry, culminating in the Water and Terrestrial Elevation Recovery Hydrosphere Mapper (WATER HM), proposed for a 2010-2020 launch time frame (Cazenave, Milly, Douville, Benveniste, Kosuth, and Lettenmaier 2003).

There are other difficulties to be met, such as the spectral characteristics of water and sediment. Pure water absorbs near infrared energy in a few millimeters, making land-water distinction easy, however remote sensing of any subsurface vegetation, such as algal blooms for example, is impossible in this

band (Campbell 2002; Wilkie and Finn 1996; Verbyla 1995; Lillesand and Kiefer 1987). Visible wavelengths can penetrate clear water to varying depths: blue (0.40 to 0.50 μm) can penetrate up to 275.0 m (902.2 ft), but is quickly scattered, red (λ = 0.65 to 0.70 μm) only penetrates to approximately 2.0 m (6.6 feet), while the blue-green region (λ = 0.48 to 0.60 μm) can penetrate upwards of 100.0 m (328.1 ft) and is not scattered like blue light (Lillesand and Kiefer 1987; Jensen 2000; Purkis, Kenter, Oikonomou, and Robinson 2002; NASA 2008). None of the water in hydrologic studies could be classified as clear, thus, other parameters interfere with collection of data beneath the surface. As sediment load increases, the spectral reflectance peak shifts to longer wavelengths, making red and near infrared useful (Campbell 2002; Verbyla 1995; Sabins 2007; Jensen 2000). Specifically, the region of "orange-scarlet" (λ = 0.58 to 0.69 μm), referenced earlier in the experiments of Ellis, can aid in typing or qualification of suspended sediments, while returns from the specific near infrared wavelength range of 0.71 to 0.88 μm can help quantify the amount of suspended sediment (Jensen 2000). However, it is important to remember that these values would only be relevant to surface water, not the full water column, where significant amounts of sediment are transported, and that this would only offer a snapshot, not a temporally significant definition of the water body.

### *Data Collection Techniques*

Landsat 7 Enhanced Thematic Mapper (ETM+) is the satellite and sensor that collected the central datasets for this research. Launched on April 15, 1999, the sensor collects six bands ranging from blue-green (0.45-0.515 μm) to shortwave infrared (2.08-2.35 μm) with 30 m spatial resolution. Enhanced Thematic Mapper also collects a thermal band (10.4-12.5 μm) with 60 m resolution, and a panchromatic band (0.52-0.9 μm) with 15 m resolution for a total of eight bands (Aronoff 2005). The grid for locating scenes consists of paths which run N-S, and rows, which run E-W. For example, path 17, row 33 would be northeast of path 18, row 34. Two scenes were used in this research; specifically path 18 rows 33 and 34 (USGS 2008).

Tabular data used with classified imagery products were collected from soil survey books, online sources, and a hydrologic engineering text (Cole 1989; Cole, Carpenter, and Delp 1985; Gorman and Espy 1975; Jones 2007; Van Houten, Childs, Teets, Estepp, and Doonan 1981; Soil Survey Division Staff, NRCS 1993; McCuen 2005; Mitasova, Brown, Hohmann, and Warren n.d.). Soil survey books provided the *K factor*, a variable in the Revised Universal Soil Loss Equation (RUSLE). The K factor is an average of soil erosion response to rainfall, surface runoff, infiltration and groundwater saturation (Renard, Foster, Weesies, McCool, and Yoder 1997; Foster 2004). The RUSLE is designed for use in agricultural applications, however the erodibility factor (K) was used for this research, as it provides a comparative scale of erosion potential (Jain, Kothyari, and Ranga Raju 2004). Another factor germane to this research is the *C factor*,

or runoff coefficient, for use in the rational method of peak discharge estimation (McCuen 2005). This is not to be confused with the C factor in the RUSLE, which is a measure of the crop management practice, such as disk plowing or fallow fields, etc. (Renard et al. 1997; Foster 2004). The runoff coefficient is a relative measure of the potential runoff of a given land cover type, where higher values equal a higher potential runoff rate (McCuen 2005; Jain et al. 2004; Mitasova et al. n.d.). A method for determining urban C factor from QuickBird classified imagery and spatial analysis produced results that were comparable to McCuen's values, the values of Jain et al., and the USACE method (Thanapura, Helder, Burckhard, Warmath, O'Neill, and Galster 2007). The roughness coefficient is a relative measure of impediment of flow over land or in a channel (McCuen 2005). In this research it was used in the former sense to show the effect of land cover types on surface runoff.

### *Image Processing Techniques*

The area of interest having been defined as the Guyandotte River watershed, it was necessary to clip the imagery to the watershed so that only the information relevant to the question could be analyzed. Several pre-processing steps are necessary before analysis can begin. When downloading imagery from the USGS and many other scientific data providers, it is possible to receive data in hierarchical data format (.hdf), wherein the imagery is compiled in a multiband file with each band available for selection in an RGB format (USGS 2008). This format lets the analyst download imagery and immediately begin analysis, and is most useful when the area of interest is encompassed by a single scene. ASTER

imagery can be delivered in this format, for example, which is easier than manually compiling each of the 14 bands. However, it is often necessary to analyze an area that spans portions of more than one image, such as in the current research (Figure 16). For this case, each band can be delivered as an individual .tiff file, and must be added into an “image stack” to be used as a multiband RGB image. This is useful when scenes must be mosaicked and/or clipped, since you can create the mosaic of two scenes, clip them, and then compile them into a multiband image. Mosaicking and color matching are much more difficult when performed on a multiband image than on a single band of information. After mosaicking and clipping, the image can be saved into a multiband image for subsequent analysis.

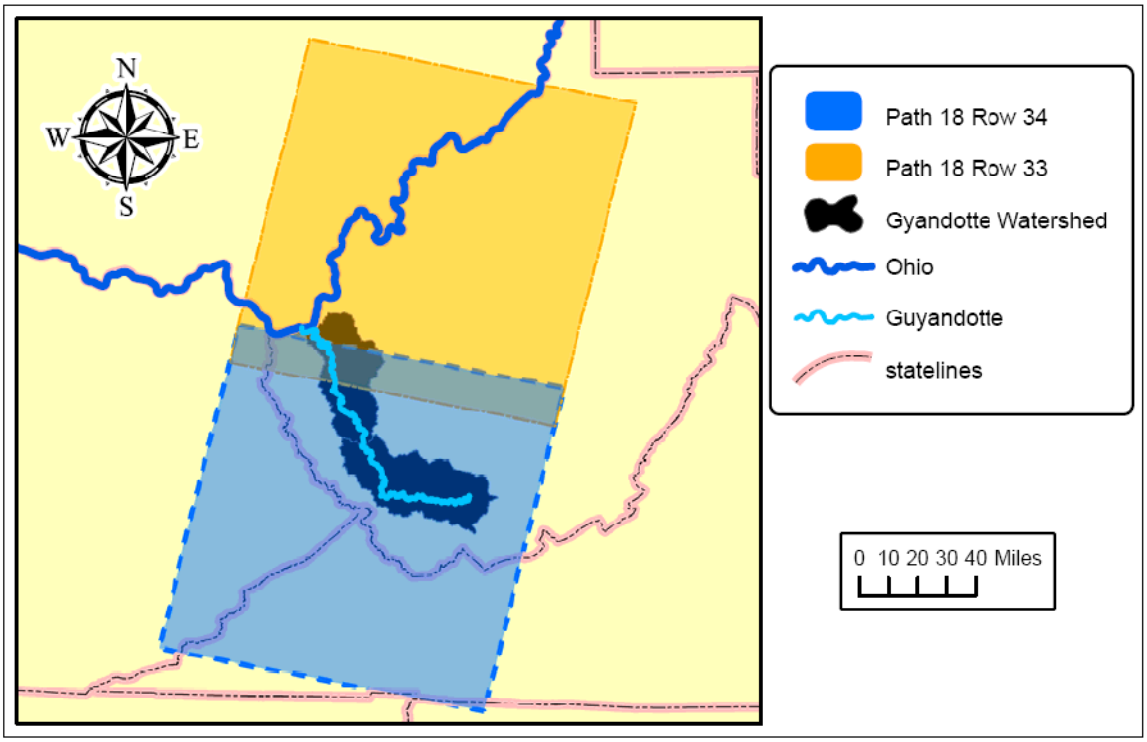


**Figure 16. Extent of Landsat 7 Scenes Used.**

The scenes were mosaicked using ESRI ArcGIS 9.2 software, and each band was saved as a .tiff file. Each of the .tiffs was then clipped to the extents of the Upper and Lower Guyandotte sub-basins using the ESRI Spatial Analyst Extract by Mask tool. The images were then imported to ER Mapper 7.1 and were saved as an image stack, or multiband RGB image. Each of the clipped bands were added to an ER Mapper algorithm as a pseudo layer, and named as its respective band. This stack was then saved as a multiband .ers file, which produces an image that has each band available in an RGB format (The Center for Earth Observation, Yale University 2006). At this point, the analysis dovetailed, with imagery being used in ER Mapper and the same imagery being used in Idrisi Kilimanjaro Edition in order to compare classification schemes of the two software packages.

The multiband .ers file was imported to Idrisi Kilimanjaro, where they were automatically created as individual .rst files for each band. If the imagery were only to be used in Idrisi, the .tiffs could have been directly imported from ArcGIS, however, exploring all avenues of import/export among the software packages can help to overcome file format issues when they arise. Any output created in Idrisi was able to be imported to ArcMap directly as the .rst file, which could be displayed, but in order to perform any processing, it needed to be saved as an ESRI grid.

Principal Components Analysis (PCA) was performed on the clipped scenes to reduce the amount of correlated or redundant data. In the instance of Landsat 7 data, there were 6 bands of information that were used, since the

thermal band 6 was omitted. The process analyzes the variance among the six bands and condenses it into one band that accounts for most of the variance of the data (Inglis-Smith 2006; Jensen 2005; Sabins 2007; Aronoff 2005; Geladi and Grahn 1996). Each subsequent component accounts for less of the variance of the image, such that the first three components usually contain most of the useful information in an image. Subsequent components contain phenomena such as noise and atmospheric interference (Campbell 2002). Principle Components Analysis was performed in Idrisi and ER Mapper to compare results.

### *Classification Techniques*

Assessment of the National Landcover Dataset (NLCD) showed that all classes necessary for this research were present. However, when the analyst classifies the imagery, he or she has more control over class decisions, such as splitting and merging of classes. If the initial classification contains enough classes, decisions can be based not only on the spectral response of materials, but also on interpretation of ancillary datasets, such as aerial photography.

Classification was performed in the Idrisi and ER Mapper software packages using unsupervised techniques. Unsupervised Classification groups pixels into classes based on brightness values (or digital numbers) across the bands of an image. This differs from supervised classification, which depends on information entered by the analyst which offers spectral signatures of relatively homogenous features. This information is known as training data. Due to the

scope of this research, it was not feasible to collect training data, thus, unsupervised classification was the best method available.

Imagery was first analyzed in Idrisi using the CLUSTER algorithm, with broad and fine generalization (Eastman 2003). Both the initial imagery and the principle components analysis imagery were classified. The best method for discerning the optimal number of classes in this case is trial and error, as defined by the analyst. Broad generalization classifications were performed with 10 and 16 classes on bands 1-5 and 7. Fine generalization was not given a class limit.

The Iterative Self Organizing Clustering algorithm (Isoclust) in Idrisi was also used on principle component and original imagery. Isoclust first analyzes all desired bands and then displays the histogram for the image. From this initial analysis, the analyst selects the number of desired classes, minimum size of classes, and the file name and location for the classified imagery. The algorithm then classifies the image according to selected parameters (Eastman 2003). Initial analysis of the histogram showed that 16 classes should be the optimal choice for both sub-basins and both principle component and original imagery.

Imagery was also analyzed in ER Mapper using the ISOCLASS module using trial and error for class numbers. The parameters to be set in the ISOCLASS module are the maximum number of iterations, maximum number of classes, the desired percent unchanged, minimum members in a class based on percentage, maximum standard deviation of class members from the class center, sampling row and column intervals, split separation value, and the minimum distance between class means (Figure 17; Earth Resource Mapping

Party 1999). Defaults were used for all but the maximum number of classes, which was set to 10 and 16 for both sub-basins, for both principle component and original imagery.

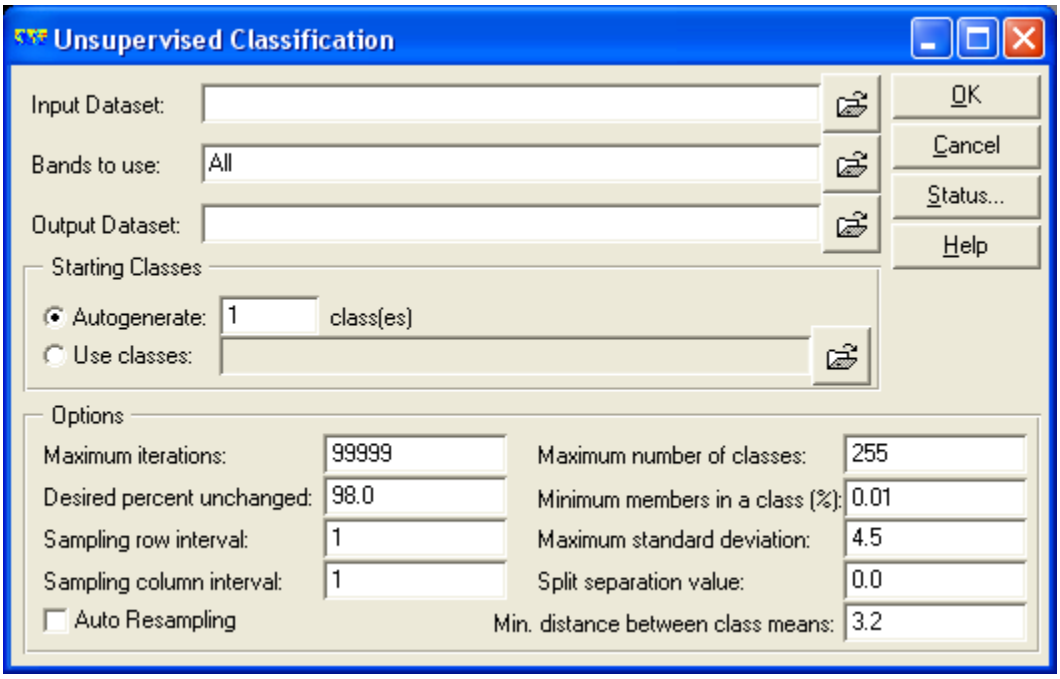


**Figure 17. Unsupervised Classification Parameters in ER Mapper 7.1**

After classification, the results required interpretation and reclassification by the analyst so that classes would be more nearly representative of conditions on the ground. While classification algorithms can be very robust, invariably they require human interpretation to clarify spectrally confusing results. Visual comparison of the classified image to aerial photography, topographic, and other thematic maps was employed to split or merge classes as needed. This hybrid of computer and human analysis is necessary to produce meaningful results.

Products of interpreted classifications were then subjected to accuracy assessment using an error or confusion matrix. This function can be performed in a number of ways, such as spreadsheet programs (Microsoft Excel or Google

Spreadsheets), or it can be performed in image processing software, such as the ERRMAT module in Idrisi (Eastman 2003). The method works on the principles of a test image and a truth image. Normally, the truth image would represent field reconnaissance or aerial photo interpretation; however the scope of the research did not allow for these methods (Franklin and Wulder 2002). Prior to assessment using the ERRMAT module, all images had to be clipped in ArcMap to match the extents of the truth image, and then imported as ASCII files back into Idrisi.

Statistics produced by the error matrix include percent correct, the kappa statistic, and calculation of errors of omission and commisison. The kappa statistic is the adjusted measure of percentage correct when chance agreement is considered, estimated by the equation: $\hat{k} = \frac{\text{Observed}-\text{expected}}{1-\text{expected}}$ (Wilkie and Finn 1996). Errors of omission and commission are complimentary, meaning one class's error of omission is another's error of commission. An example of an error of omission from this research would be the assignment of an area of pasture on the ground to the low intensity residential class in the imagery, thus omitting the pixels from the class in which they should have been included (Aronoff 2005). The pixels erroneously added to the low intensity residential class would be an example of an error of commission with respect to the residential class, since the number of pixels in the class is incorrectly inflated. Both indices are important, since classification and interpretation could produce an image that has minimal errors of omission, and due to excessive commission still be a very inaccurate image.

### *Image Data Manipulation and Spatial Analysis Techniques*

Classified image data was integrated into geographic information systems for analysis. To accomplish this, imagery was imported from Idrisi to ArcGIS and saved as an ESRI GRID. Fields were added to the attribute tables of the rasters for the roughness coefficient and the C factor (runoff coefficient) for each land cover class (McCuen 2005). Soil polygon shapefiles were downloaded from the USDA-NRCS for all of the counties in the watershed except Raleigh, which was not available (USDA-NRCS 2008). The shapefiles were clipped to the Guyandotte watershed boundaries, the K factor (erodibility factor in RUSLE) added to each soil unit, and the vector file was rasterized (Cole 1989; Cole et al. 1985; Gorman and Espy 1975; Jones 2007; Van Houten et al. 1981; Renard et al. 1997). A 30 m digital elevation model (DEM) of West Virginia was clipped to the Guyandotte watershed and slope was calculated using percent rise and classified into ten classes (West Virginia GIS Tech Center 2007). Rasters were then added into a suitability model that used thresholds to highlight probable sources for increased sedimentation. The thresholds were based on each relative scale in order to highlight factors that were considered favorable to increased sedimentation. The resulting Boolean rasters were combined using AND operators to complete the analysis (Figure 18; Childs, Kabot, Murad-al-shaikh 2004; Jain et al. 2004; Price 2006).

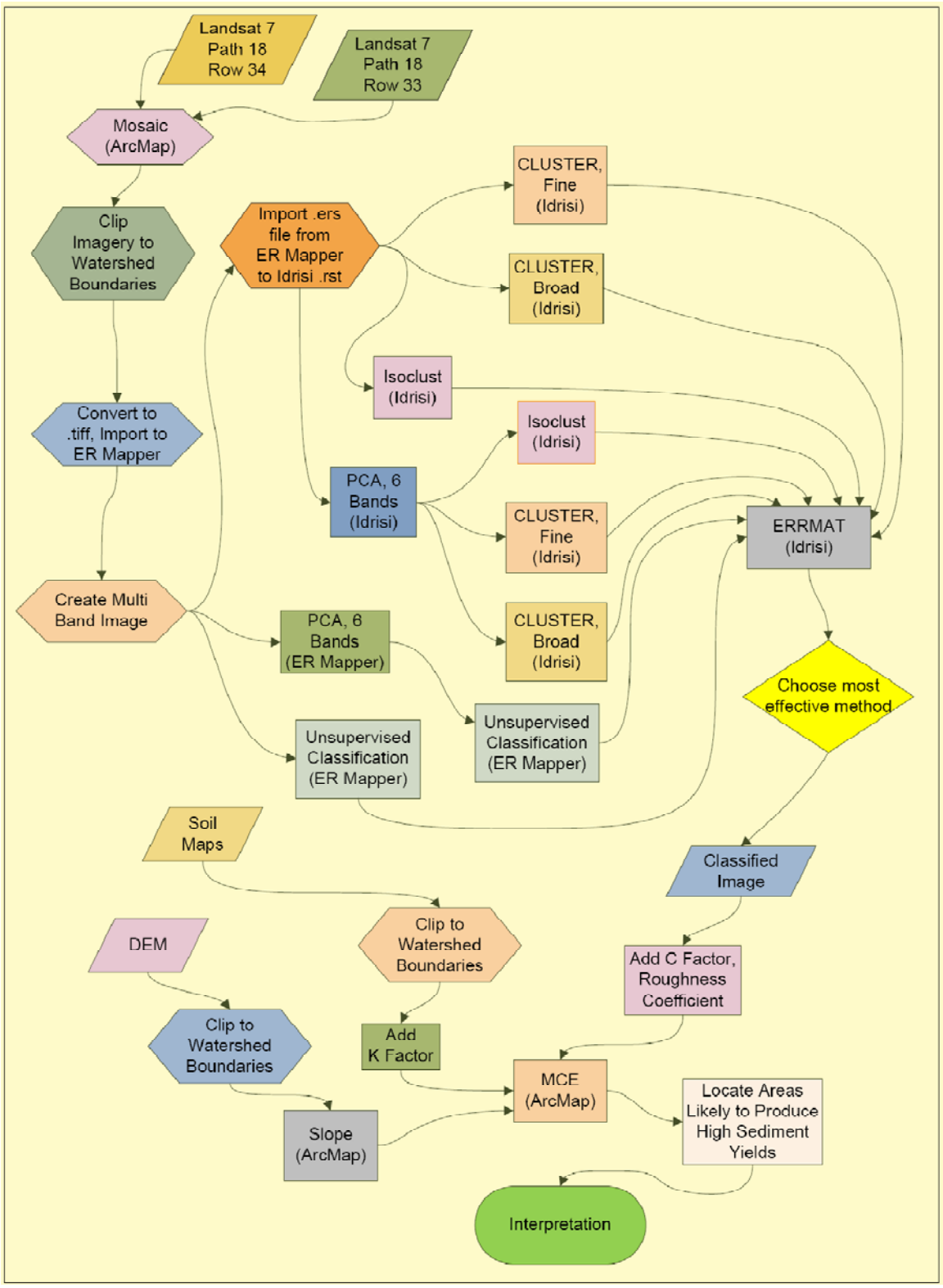


**Figure 18. Analytical Processes.**

# CHAPTER III

## Results and Discussion

### *Overview*

Previous research produced classified images for the upper and lower sub-basins of the Guyandotte watershed with the goal of finding the most appropriate method of classification for the research question. Methods ranged from aesthetic and visual interpretation to statistical comparison. The most important of these factors was based on accuracy assessment, or the comparison of the classification to perceived ground conditions. Ideally, this comparison is based on ground truthing field visits to a random sample of cover types within the classified area, however, the scope of this research necessitated modification of this method. Following selection of classified imagery, a roughness coefficient and C factor (runoff coefficient) were both applied to each class. The K (erodibility) factor was applied to the merged and clipped soil shapefile, which was then rasterized. A slope raster was created from the 30 m digital elevation model. Finally, a suitability model was created with the rasters to identify areas that were most likely to adversely affect the sediment yield.

### *Classification Results*

Principal components images produced by Idrisi and ER Mapper were very similar in most respects (Figures 19 and 20). However, one important difference was noted in ER Mapper: when the components were composited in an RGB image, Component 2 contained information that highlighted hillshade effects from the sun angle at the time of collection. Replacing this component with another reduced the visual differentiation between land cover classes in light

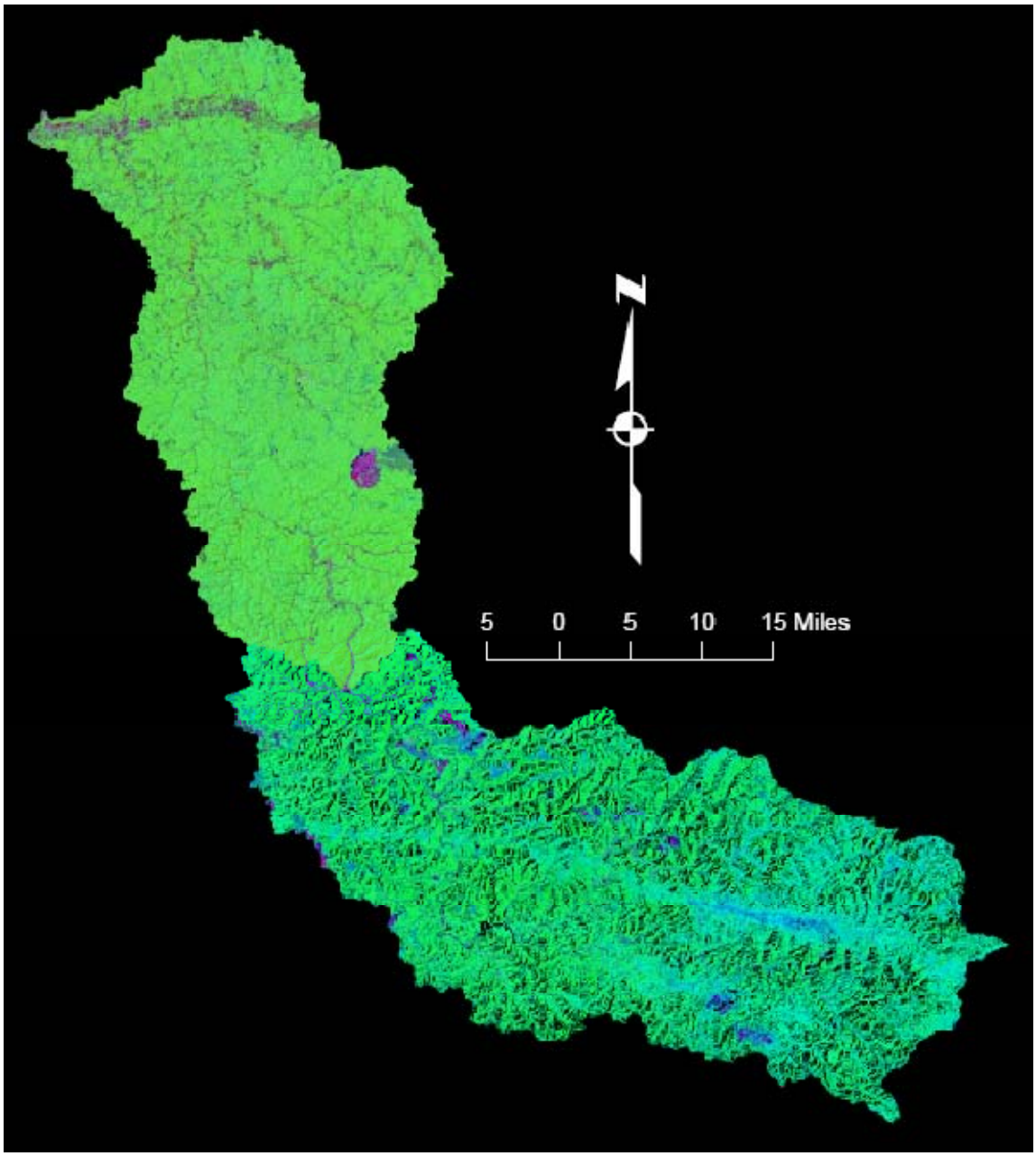


**Figure 19. Principle Components 1, 2, and 3 as RGB Image (ER Mapper).**

and shadow. This difference could be very useful for classification in mountainous terrain, since sun angle will always play some role in confusion of classification. Through trial and error, the combination that seemed most useful was principle components 1, 3, and 5 (Figures 21 and 22). Through visual inspection, this combination seemed to show the least unwanted variation (valley

shadows). Idrisi did not exhibit this ability, as all components had a high amount of hillshade confusion.

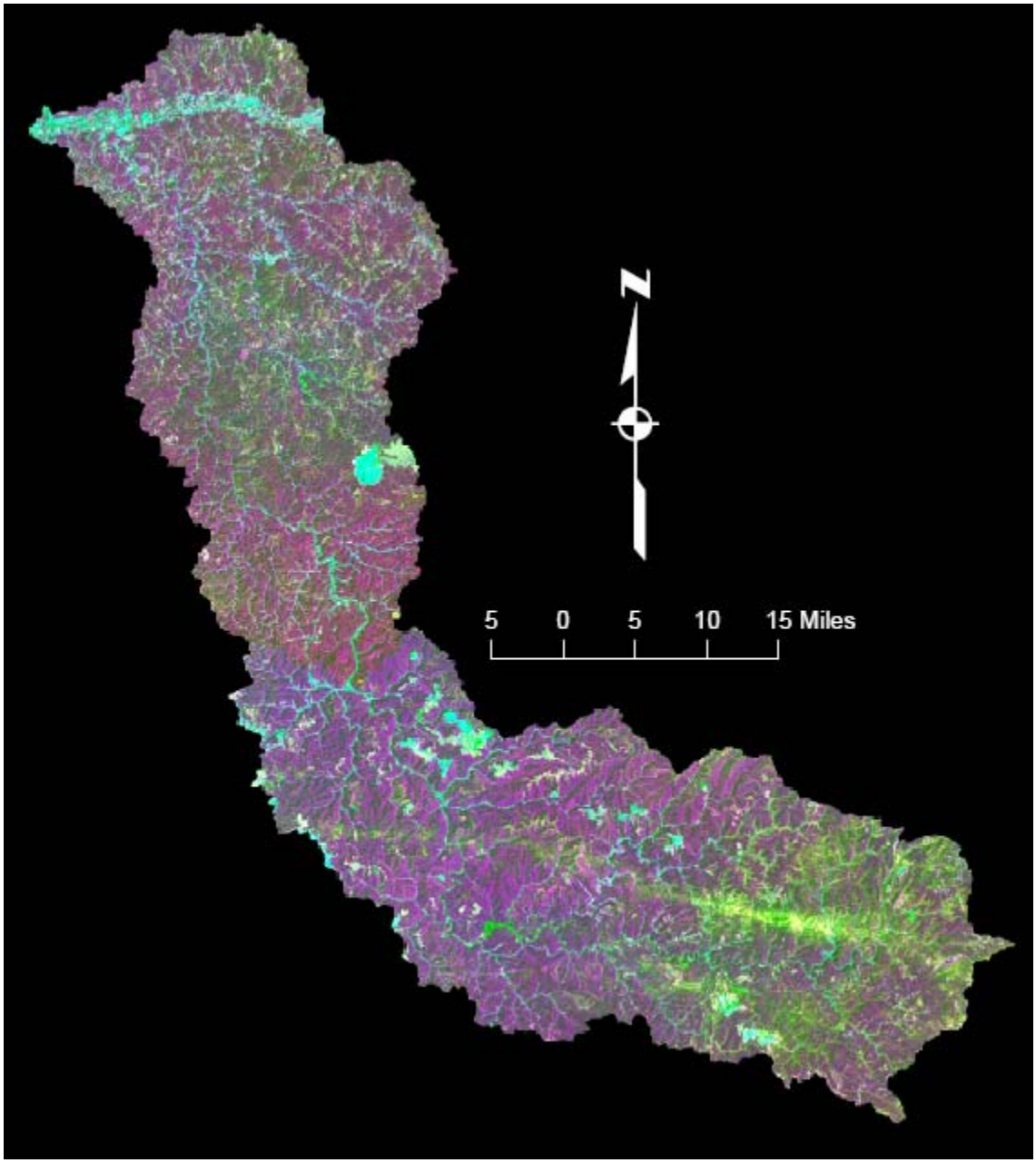


**Figure 20. Principle Components 1, 2, and 3 as RGB Image (Idrisi).**

Unsupervised Classification of the sub-basin images in ER Mapper (ISOCLASS) set to 10 classes produced images that showed differentiation between water, urban classes, various vegetation, and extensive bare-earth

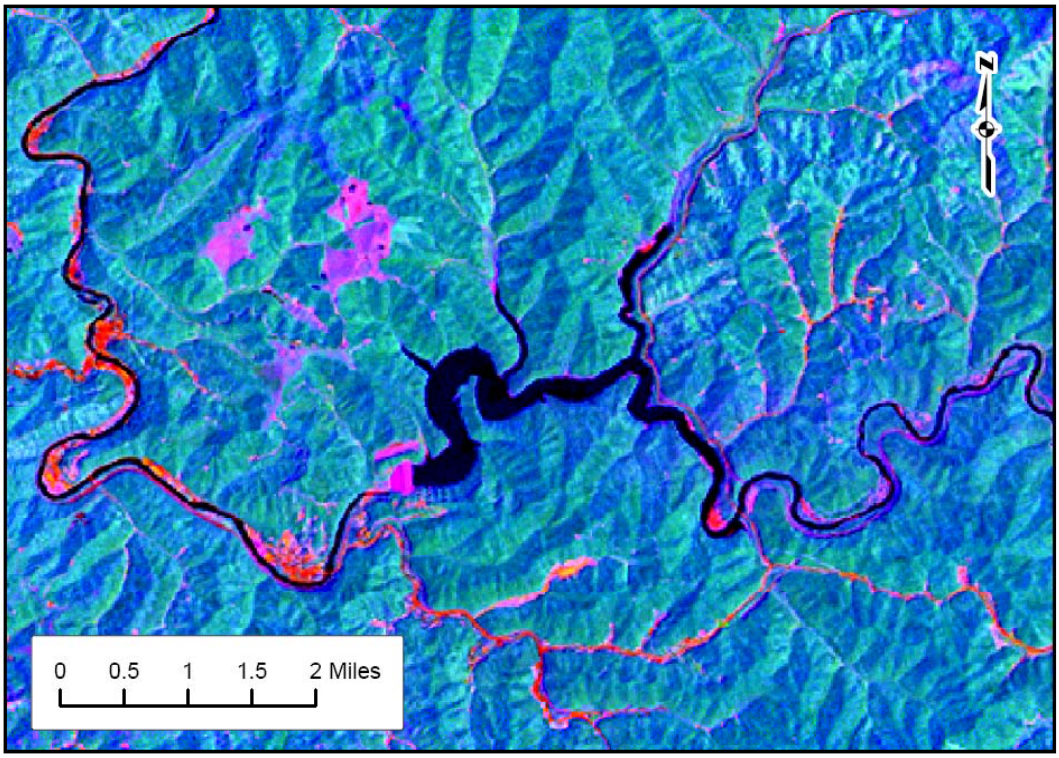


**Figure 21. Principle Components 1, 2, and 3 as RGB Image (ER Mapper).**

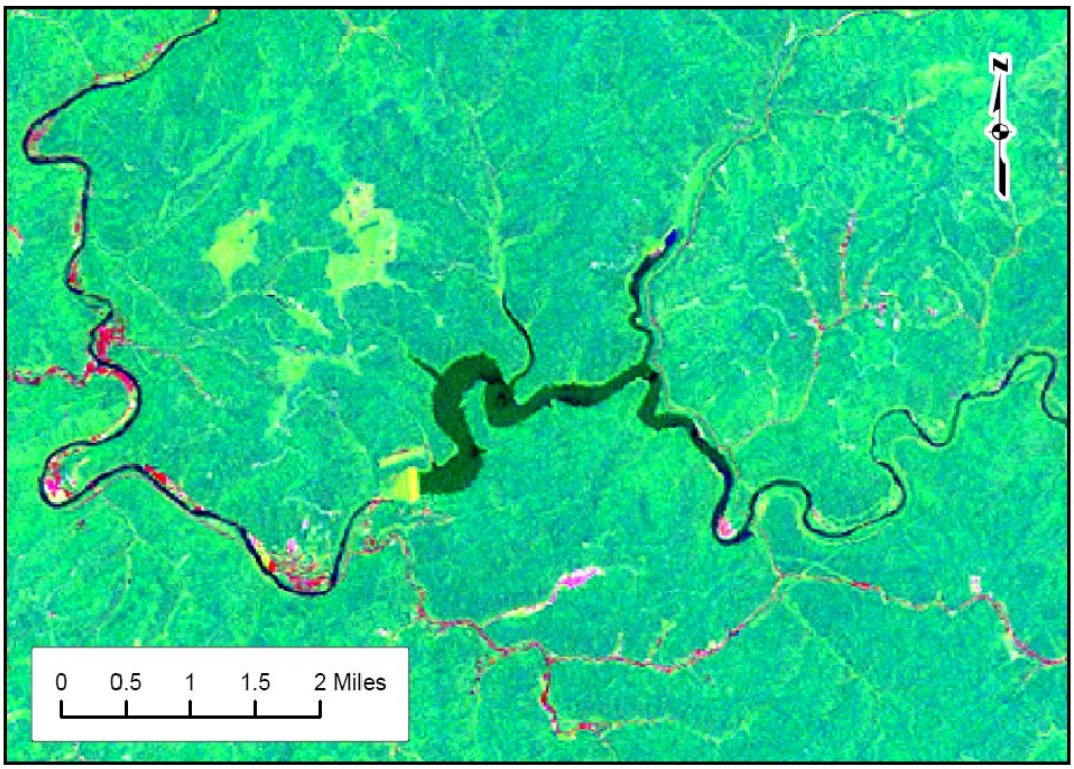


**Figure 22. Principle Components 1, 3, and 5 as RGB Image (ER Mapper).**

activities (Figure 23). Some variation, such as incorrect classification of water in the south of the Upper Guyandotte sub-basin, or the splitting of forest classes in valleys was attributed to valley shadows (Figure 24, yellow). The principle components images that were classified by this module de-emphasized valley shadows, however the ISOCLASS module grouped standing water together with much of the countryside, probably due to transpiration (Figure 25, yellow).

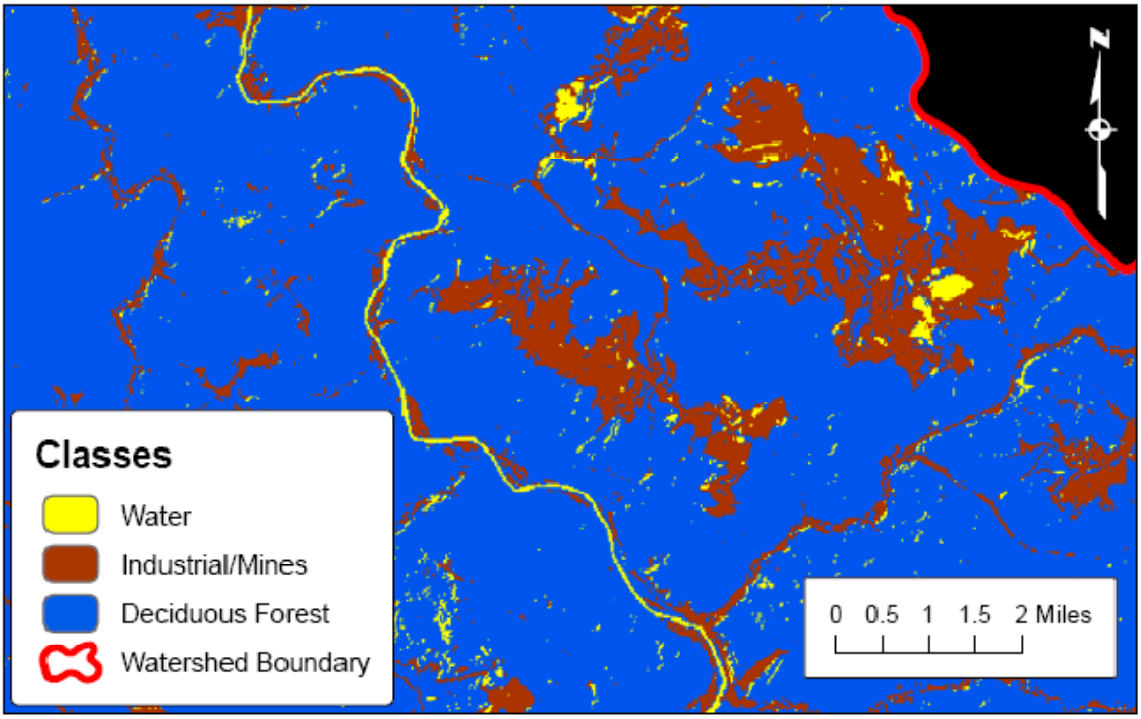


**Figure 23. ISOCLASS Highlighting Industrial Activity/Mining and Water.**

Unsupervised Classification of imagery in Idrisi (CLUSTER, Fine and Broad) with 10 classes produced good results in the Lower Guyandotte sub-basin, while problems with confusion from shadow, moisture, and urban or industrial areas were rampant in the Upper Guyandotte (Figures 26 and 27). CLUSTER with Fine Generalization differentiated well among most classes; however water and shadow were still frequently confused (Figure 28).

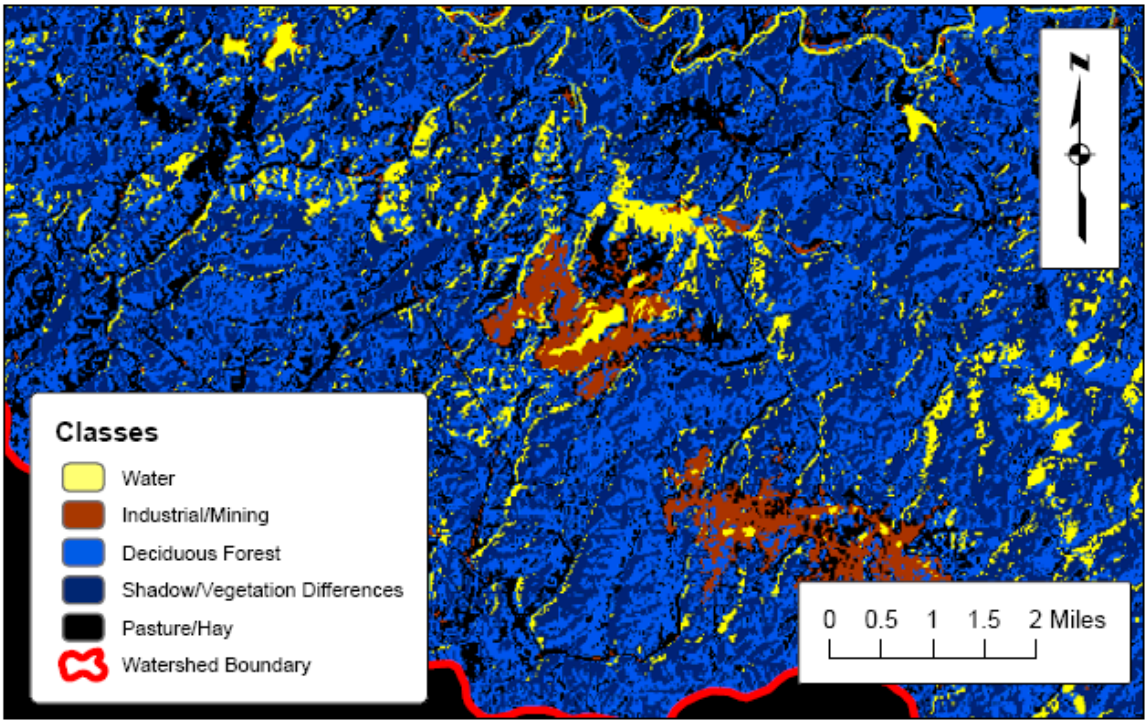


**Figure 24. ISOCLASS Highlighting Valley Shadows or Vegetation Differences.**

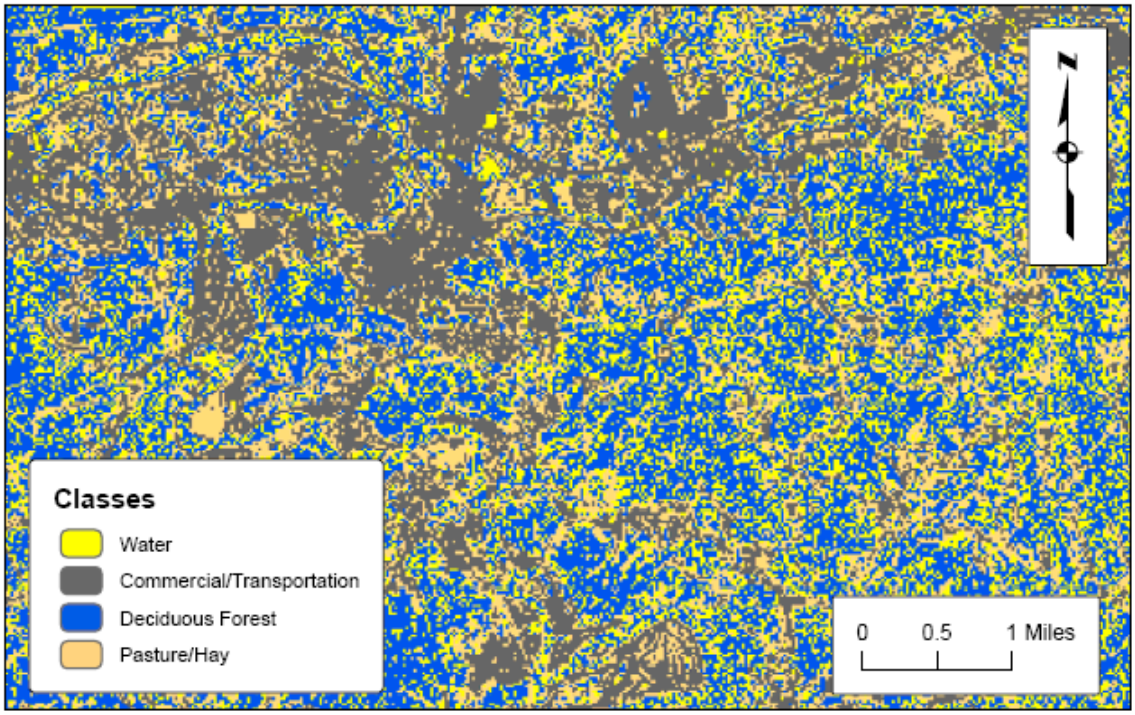


**Figure 25. ISOCLASS Principle Components Image Showing Mixed Pixels Due to Transpiration.**

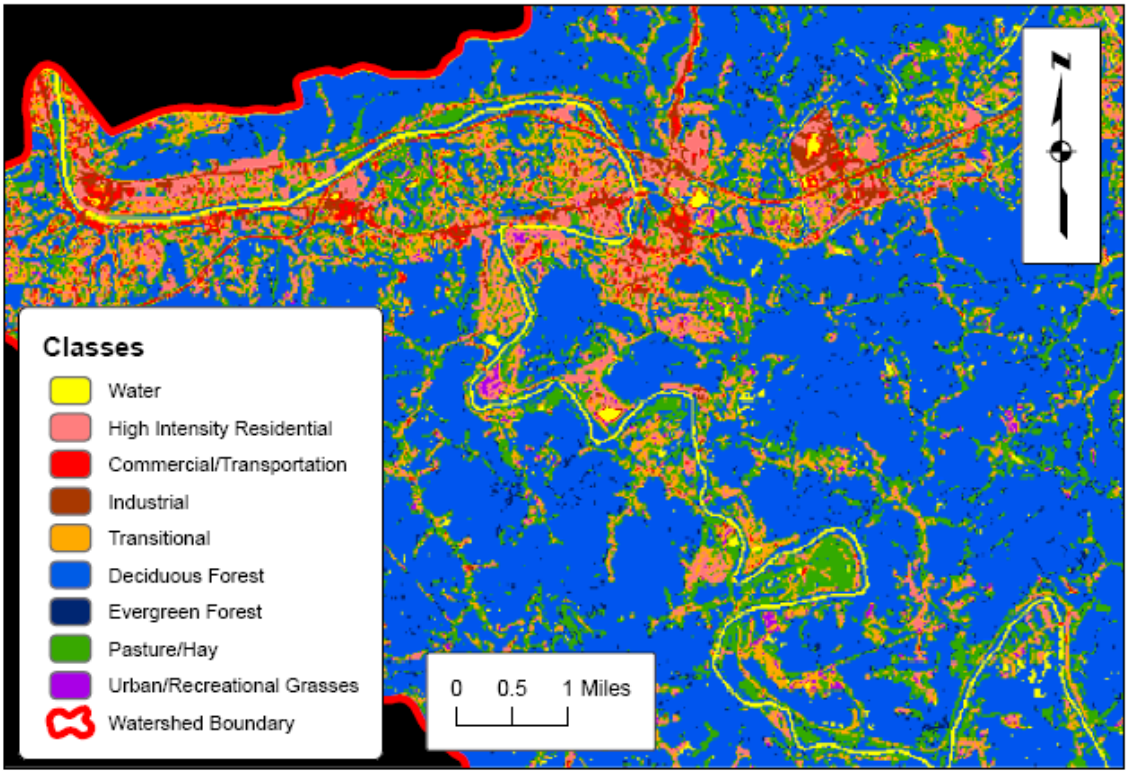


**Figure 26. CLUSTER, Broad Generalization. Lower Guyandotte Sub-Basin.**

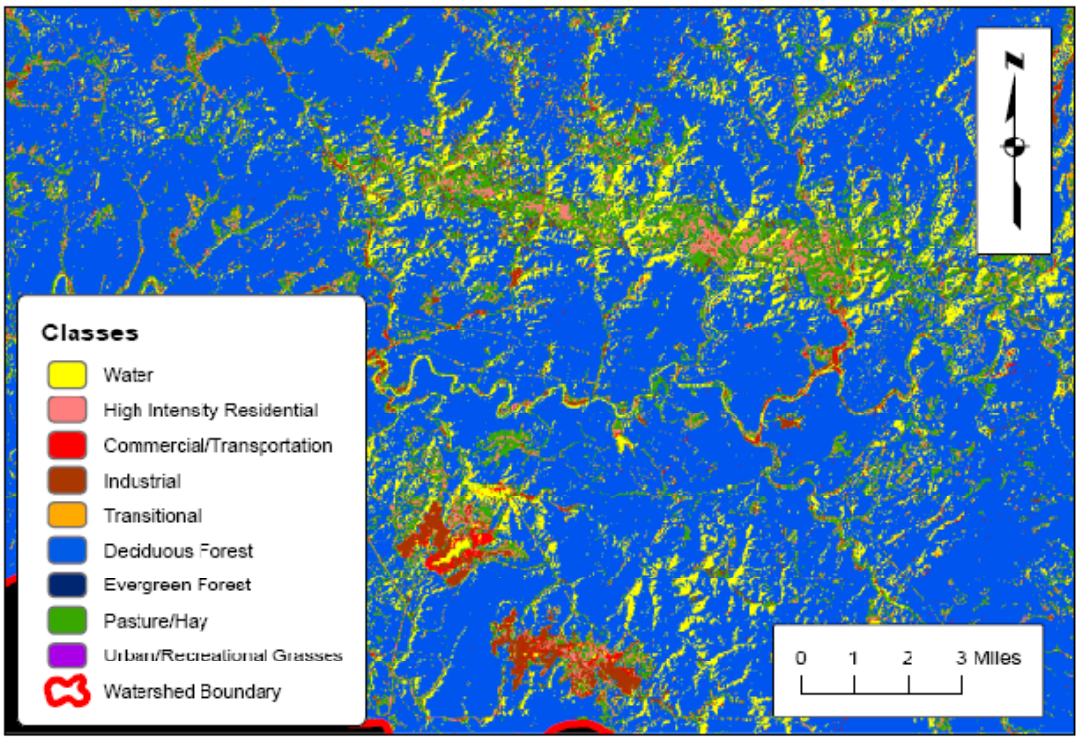


**Figure 27. CLUSTER, Broad Generalization. Mixed Pixels in Upper Guyandotte Sub-Basin.**

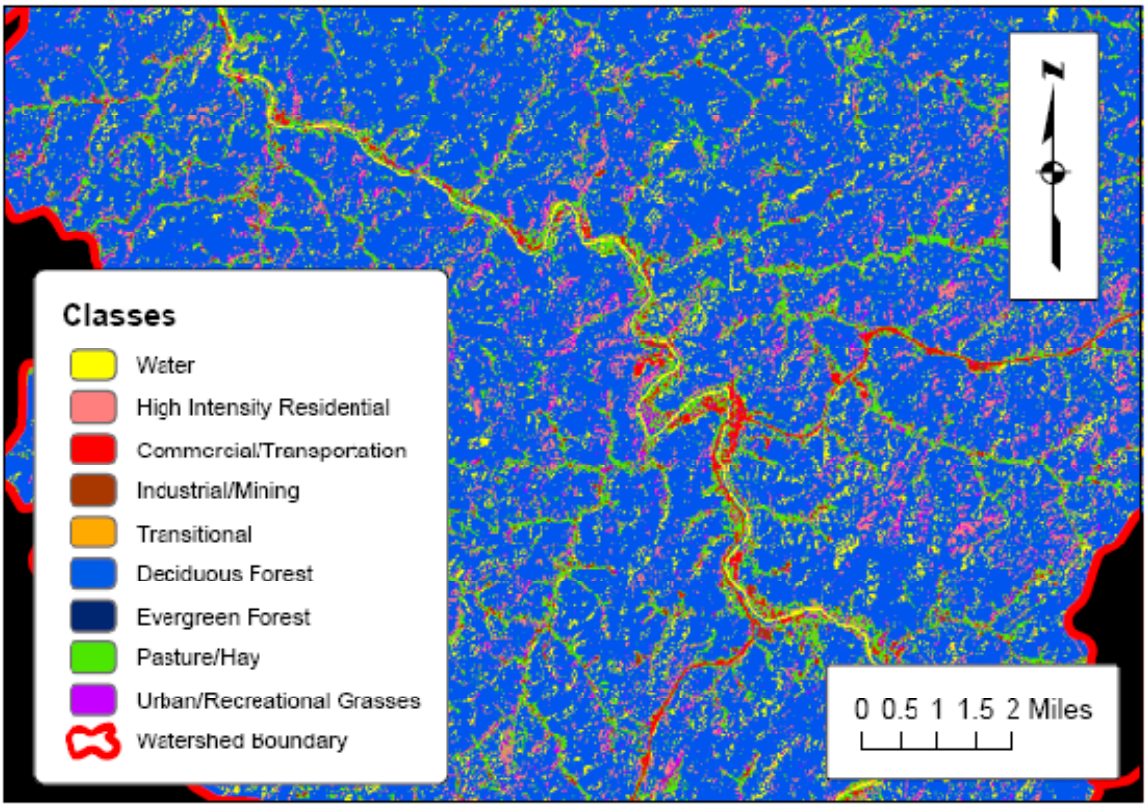


**Figure 28. CLUSTER, Fine Generalization. Mixed Pixels in Lower Guyandotte Sub-Basin.**

Visual assessment of the classification schemes shows that the CLUSTER module with Broad generalization set to produce 10 classes proved to be the best, with ISOCLASS in ER Mapper being very similar. Due to the promising results produced by the CLUSTER and ISOCLASS modules, images were also produced by each for bands 1-5 and 7 with 16 classes. These images were superior to the 10-class products since they offered the analyst more interpretive leeway when compared with higher resolution aerial imagery. Differentiation of classes in the urban area in the Teays Valley between Barboursville and Huntington was very good when compared to 2 ft (61 cm) pixel orthophotos (Figures 29 and 30).

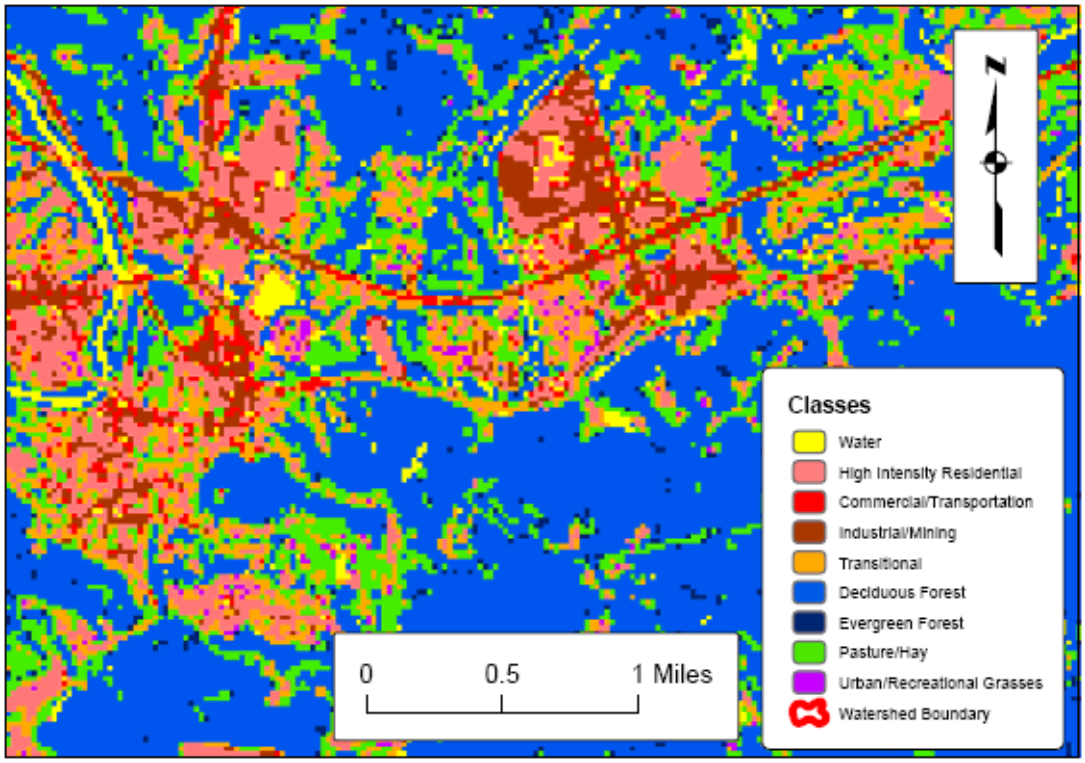


**Figure 29. CLUSTER, Broad Generalization, 16 Classes. Differentiation of Urban Area.**


**Figure 30. SAMB Barboursville NE, SE and Milton NW, SW DOQQs. 2003 (WVGISTC 2008).**

The Iterative Self Organizing Clustering (Isoclust) algorithm returned very good results, although confusion among water and shadow was evident (Figure 31, gold). The Isoclust module using the principle component images differentiated urban, mining, water, and transportation from surrounding vegetation; however these four classes were combined into one, though there seemed to be less confusion from transpiration (Figure 32, yellow). A primary focus of this research is to isolate industrial activities from other classes, therefore this was an unacceptable shortcoming.

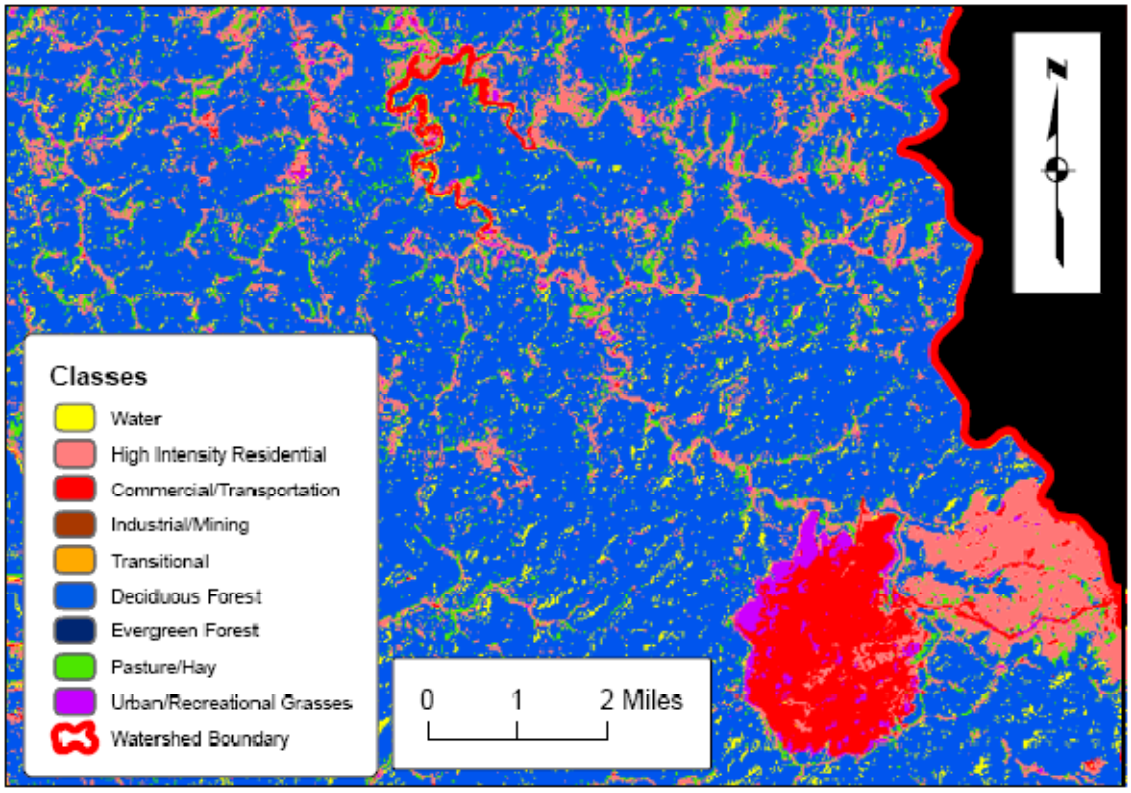


**Figure 31. Isoclust. Water and Mining Combined in Single Class.**

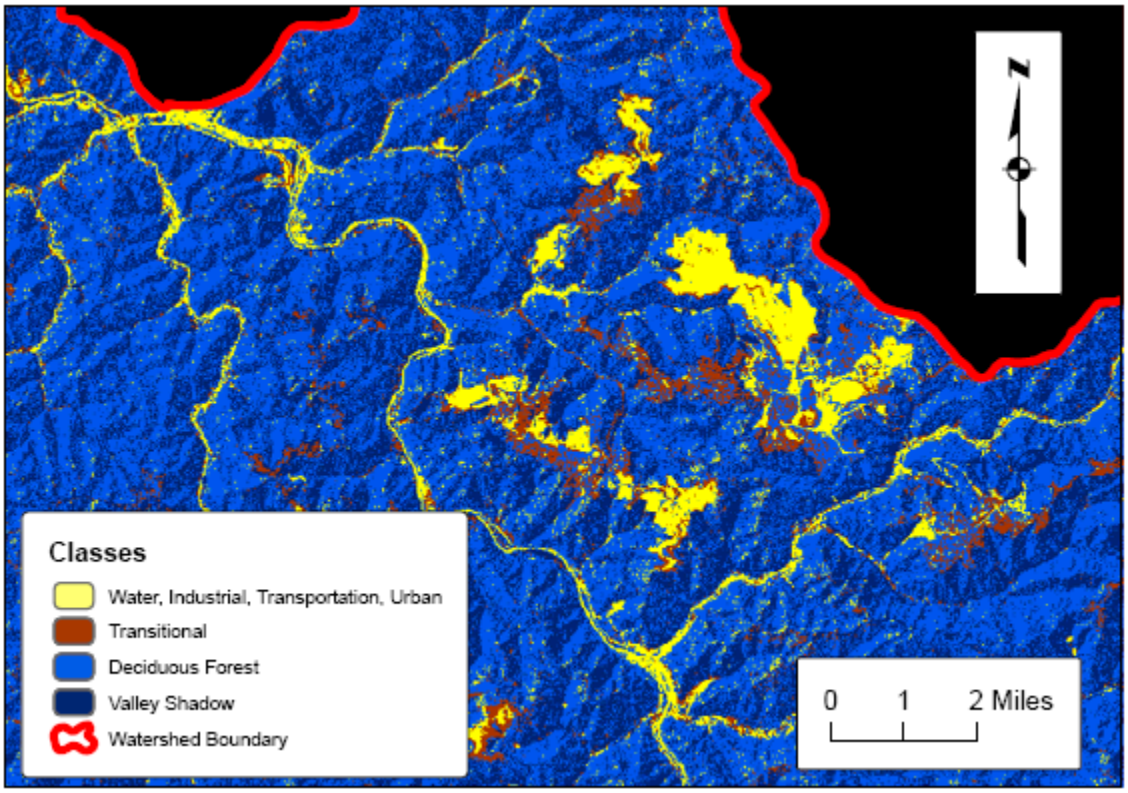


**Figure 32. Isoclust of Principle Components Image. Class Containing Several Cover Types.**

After visual analysis and comparison, the 16 class images produced by the CLUSTER module were selected to continue with the research. The final images of 16 classes were interpreted and reclassified using aerial photography and thematic maps. The final result was imagery of 10 classes with descriptions similar to the classification scheme used by the National Landcover Dataset (Anderson et al. 1976). Final classes are summarized in Table 3.

| Class (NLCD Number) | Class (NLCD Name) |
|---|---|
| 11 | Open Water |
| 21 | Low Intensity Residential |
| 22 | High Intensity Residential |
| 23 | Commercial/Industrial/Transportation |
| 32 | Quarries/Strip Mines/Gravel Pits |
| 33 | Transitional |
| 41 | Deciduous Forest |
| 42 | Evergreen Forest |
| 81 | Pasture/Hay |
| 85 | Urban/Recreational Grasses |

**Table 3. Classes of Final Imagery.**

### *Accuracy Assessment Results*

The classified images were subjected to accuracy assessment using the ERRMAT module in Idrisi, which produces an error matrix. Prior to assessment, all images had to be clipped in ArcMap to match the extents of the NLCD, and then imported as ASCII files back into Idrisi. After interpretive reclassification into category number values that would match the NLCD classification scheme, the images were each compared to the NLCD. Each comparison produced a table of vital statistics. The Lower Guyandotte CLUSTER (broad, 16 classes) image when compared to the NLCD was 38.8% “correct”. If this were from comparison with field reconnaissance, this figure would not be very good. At best, the classifications produced by this research do not agree well with the NLCD. For this comparison, the kappa statistic, $\hat{k}$, = 0.2434, meaning that this classification achieved accuracy 24% better than chance assignment of pixels. Errors of omission and commission are also included in the matrix (Tables 4 and 5). Using this example, the most successful class identification was of Deciduous Forest (41), with an approximate 87% probability that forest on the map will be forest in

the field (Table 4). Also, of Deciduous Forest on the landscape, 86% was classified correctly (Table 5; Aronoff 2005).

| Class | Pixels per Class (BRCL16) | Error *C* per Class |
|---|---|---|
| 0 (*Null*) | 1808557 | 1.0000 |
| 1 | 6121 | 1.0000 |
| 11 | 23859 | 0.9283 |
| 22 | 44991 | 0.9986 |
| 23 | 4944 | 0.8206 |
| 32 | 12179 | 0.9745 |
| 33 | 88431 | 0.9945 |
| 41 | 1702665 | 0.1302 |
| 42 | 48932 | 0.9944 |
| 81 | 188466 | 0.7641 |
| 85 | 13121 | 0.9985 |

**Table 4. Errors of Commission per Class.**

| Class | Pixels per Class (NLCD) | Error *O* per Class |
|---|---|---|
| -9999 (*Null*) | 1808557 | 1.0000 |
| 11 | 8969 | 0.8093 |
| 21 | 25573 | 1.0000 |
| 22 | 163 | 0.6012 |
| 23 | 11928 | 0.9256 |
| 32 | 8120 | 0.9617 |
| 33 | 3626 | 0.8657 |
| 41 | 1724753 | 0.1413 |
| 42 | 19373 | 0.9858 |
| 43 | 142815 | 1.0000 |
| 81 | 160616 | 0.7231 |
| 82 | 26659 | 1.0000 |
| 85 | 692 | 0.9711 |
| 91 | 249 | 1.0000 |
| 92 | 173 | 1.0000 |

**Table 5. Errors of Omission per Class.**

The most successful and appropriate classifications proved to be those produced with CLUSTER (broad, 16 classes) in both sub-basins, though the ISOCLASS module (ER Mapper) was similar. For the purposes of this research, these images provide the level of differentiation necessary to discern the sources of increased sediment load for the study area (Figure 33).

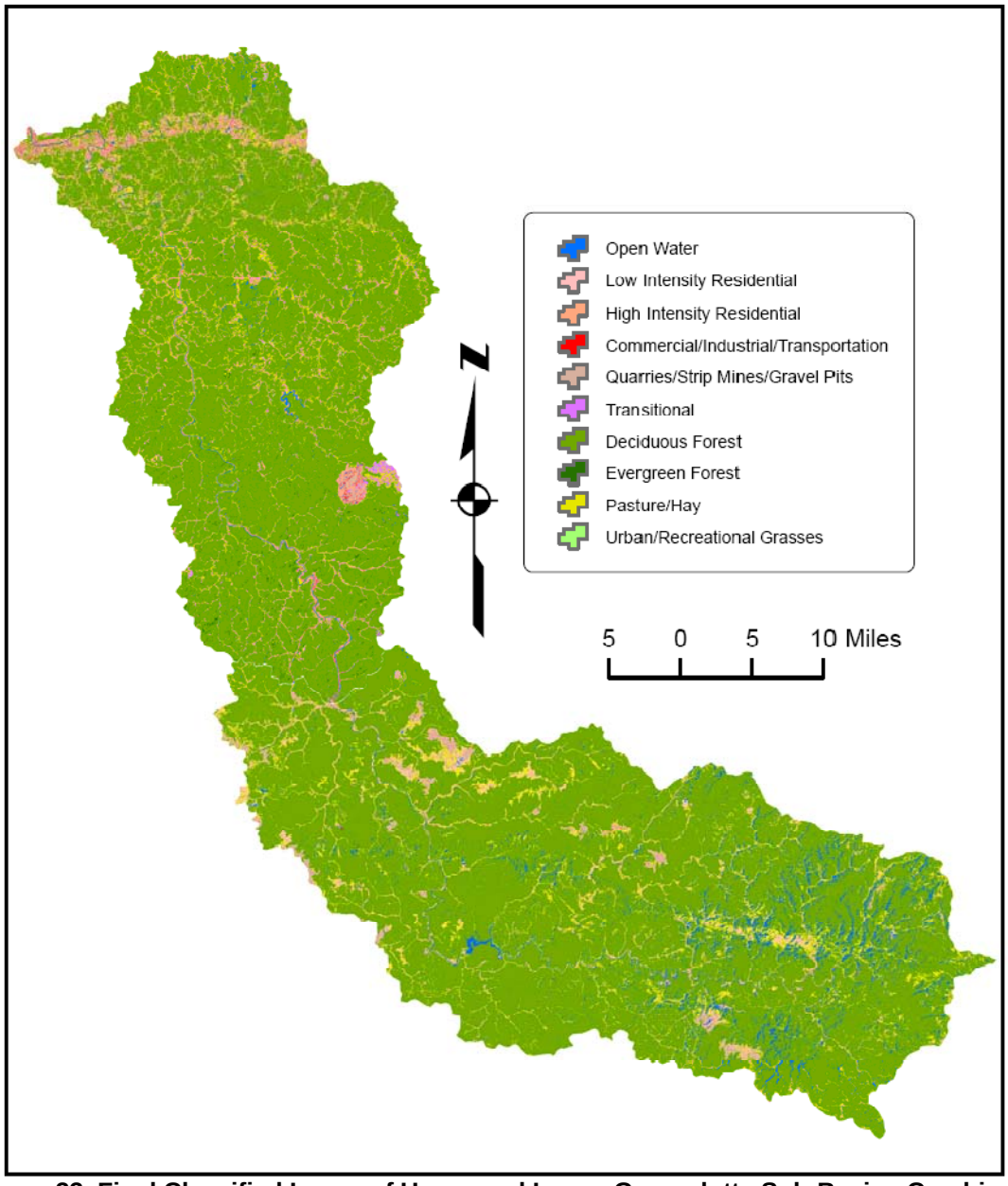


**Figure 33. Final Classified Image of Upper and Lower Guyandotte Sub-Basins Combined.**

### *Image Data Manipulation and Spatial Analysis Results*

The C factor derived from various sources was applied to each class of the selected classified imagery. A roughness coefficient was added to each class as an alternative relative measure of impediment of flow by land use class. The K factor was added to the merged and clipped soils shapefile, which was subsequently rasterized. In addition, a 30 m resolution digital elevation model was used to create a percent-rise slope raster for subsequent analysis.

The C factor (runoff coefficient) was added to the attribute table of the classified images. Larger C values reflect increased runoff potential, which means higher potential for sediment sources. Drawing from a variety of sources, reliable median values were obtained for all of the identified classes (Jain et al. 2004; Thanapura et al. 2007; McCuen 2005). Visual inspection of the values validates the idea that industrial and bare earth activities will provide increased runoff, which will provide increased erosive power, and increased sedimentation (Table 6). Impervious surfaces (commercial/industrial/transportation) had a value of 0.85, while heavy industrial (quarries/strip mines/gravel pits) had a value of 0.75, and light industrial (transitional) had a value of 0.65. Residential areas ranged from low intensity, with a value of 0.35, to high intensity, with a value of 0.50. Forest (deciduous and evergreen) was estimated at 0.12. The pasture/hay class was estimated at 0.31, and the urban/recreational grasses class was estimated at 0.20. Water was not estimated by any source, thus it was reasoned that open water would approach 1.00.

| Class (NLCD Number) | Class (NLCD Name) | Runoff Coefficient |
|---|---|---|
| 11 | Open Water | 1.00 |
| 21 | Low Intensity Residential | 0.35 |
| 22 | High Intensity Residential | 0.50 |
| 23 | Commercial/Industrial/Transportation | 0.85 |
| 32 | Quarries/Strip Mines/Gravel Pits | 0.75 |
| 33 | Transitional | 0.65 |
| 41 | Deciduous Forest | 0.12 |
| 42 | Evergreen Forest | 0.12 |
| 81 | Pasture/Hay | 0.31 |
| 85 | Urban/Recreational Grasses | 0.20 |

**Table 6. Runoff Coefficient per Class.**

Manning's roughness coefficient was used as an alternative relative measure of runoff potential and indirectly, of potential erosive power. The coefficient measures the surface roughness ranges for various land cover types. It is suggested to use the mean of each range unless a specific reason is stated (McCuen 2005). The lower the value, the lower the surface roughness, making passage of water easier and faster. In this research, the coefficient was used for all land cover types in the watershed. In hydrologic engineering practices, Manning's coefficient is used for estimation of flow within the channel, however, the resolution of available imagery and available channel morphology data did not allow differentiation of channel characteristics. Therefore, for the channels themselves, or the open water class, the value was estimated at 0.031, or Manning's coefficient for major streams. Due to the resolution of Landsat imagery, major streams are the main constituent of open water that would be present. The low intensity residential class was interpreted to fall in the dense grass range of 0.240. The high intensity residential class was assigned the short grass value of 0.150. The commercial/industrial/transportation class was given

the value for asphalt, 0.012. The quarries/strip mines/gravel pits class was given the recommended value for bare land, 0.010. The usually spatially adjacent transitional class was given the value for short grass, or 0.150, since it was reasoned that this usually was a class of poorly maintained reclaimed grassy land. The deciduous forest class was interpreted to be forest with dense underbrush, which received the value of 0.800. Evergreen forest was interpreted to have lighter underbrush, which was given a value of 0.400. The pasture/hay class was interpreted to resemble Bermuda grass, which was afforded a value of 0.410. Urban and recreational grasses was estimated to belong to the dense grass value of 0.240. All values were taken from McCuen's *Hydrologic Analysis and Design* textbook and applied through user interpretation of land cover types (Table 7). As a result, these numbers are considered somewhat subjective.

| Class (NLCD Number) | Class (NLCD Name) | Manning's Roughness Coefficient |
|---|---|---|
| 11 | Open Water | 0.031 |
| 21 | Low Intensity Residential | 0.240 |
| 22 | High Intensity Residential | 0.150 |
| 23 | Commercial/Industrial/Transportation | 0.012 |
| 32 | Quarries/Strip Mines/Gravel Pits | 0.010 |
| 33 | Transitional | 0.150 |
| 41 | Deciduous Forest | 0.800 |
| 42 | Evergreen Forest | 0.400 |
| 81 | Pasture/Hay | 0.410 |
| 85 | Urban/Recreational Grasses | 0.240 |

**Table 7. Manning's Roughness Coefficient per Class.**

The K factor was derived from the table titled *Physical Properties of the Soils* in the soil surveys of Boone, Cabell, Kanawha, Lincoln, Putnam, and Wyoming County (Cole 1989; Cole et al. 1985; Jones 2007; Van Houten et al. 1981; Wolf 1988 and 1994). A soil survey was not available for Mingo and Logan

counties, but a shapefile for soils was available, and most of the soils were similar to surrounding counties. The soil survey for Fayette and Raleigh counties was available, however a shapefile for Raleigh was not, thus it had to be excluded (Gorman and Espy 1975). The Raleigh County section of the watershed accounted for 63,459 acres (25,681 ha), 99 square miles (256 sq km), or approximately 6% of the total watershed.

The range for the K factor was 0.10 to 0.43 (Cole 1989; Cole et al. 1985; Jones 2007; Van Houten et al. 1981; Wolf 1988 and 1994). Soils for which a K factor could not be found (n=11, or 6% of the 181 total) were given a value of 0 (Appendix A). After the K factor was added, the shapefile was symbolized to show and inspect the spatial variation of values (Figure 34). The shapefile was then converted to a raster with 30 m pixels to coincide with the 30 m resolution of the classified imagery.

A 30 m digital elevation model (DEM) was clipped to the watershed and analyzed to produce a percent rise, or rise over run, slope raster. A slope of 100 percent would mean that for every unit traveled horizontally, a unit would also be gained vertically, yielding a 45% angle. Therefore, slopes greater than 100% were possible. The range of percentage of slope in the Guyandotte watershed was 0 to 191.3%. The highest values were in the Mingo and Logan county sections, and in the headwaters in Wyoming County (Figure 35).

Suitability analysis was performed in ArcGIS 9.2 by creating thresholds for each of the datasets. Thresholds were based on each relative scale, creating Boolean rasters (1 and 0) of suitability for the criteria. These rasters were then

combined using an AND operator to show the coincidence of favorable factors for an increase in sediment output.

The runoff coefficient, or C factor, was considered to be favorable to increased sedimentation at values greater than or equal to 0.50. This would include areas of high intensity residential, commercial/industrial/transportation, quarries/strip mines/gravel pits, transitional, and open water (Table 6). These results were useful for adding interpretive numeric values to medium resolution imagery, however, they may not be as effective when using higher resolutions. The conditional map algebra statement used to create a suitability raster was stated as: *CON (guy_recl >= 0.5, 1)* where *guy_recl* is the name of the raster containing C factor data. The output was called *c_facs.*

Manning's roughness coefficient presented an alternative value for the principle of impediment of overland flow. Values lower than 0.200 were considered to be favorable to increased sediment yield (Table 7). This coefficient, while similar to the C factor, showed more variation in forest cover types, which is considered more nearly correct. This coefficient also had a specific value for bare land, which was used for the quarries/strip mines/gravel pits class. Despite more accurate values for portions of the research question, the selected thresholds highlighted identical land cover classes, making them redundant for this analysis, thus no additional suitability raster was necessary.

The K factor for soil erodibility exhibited a scale of 0.10 to 0.43 (Figure 34; Appendix A). Values of 0 were accepted for soils that had no K factor available in the literature, and Raleigh County was excluded from this analysis. While many

factors affect measurement of erosion, this coefficient was interpreted to show that lower values showed higher erosion potential (Cole et al. 1985). A K factor of 0.24 was selected as the threshold, and values below or equal to this were extracted. These values were indicative of the top layer of soils, since surface runoff was the focus of research, ranging from the surface to 13 to 48 cm (5 to 19 in). A separate suitability raster was not created for this layer, rather, the suitability was extracted during the final analysis.

Slope was calculated from a 30 m digital elevation model (DEM) to show percent rise throughout the watershed (Figure 35). The steepest slopes were found in Mingo and Logan counties, along the Guyandotte River channel in Wyoming County, and in the headwaters of the watershed in eastern Wyoming County. Slopes were considered steep around 50% rise, which favored much of the upper sideslopes of the southern part of the watershed (Figure 36). A separate suitability raster was not created for this layer, and as the previous raster, the suitability was extracted during the final analysis.

All factors were combined using the map algebra module in ArcGIS Spatial Analyst. The conditional statement for the suitability model of potential erosion was stated as:

*con (slopeguy >= 50 and soil <= 0.24 and c_facs == 1, 1)*

where *slopeguy* is the slope raster, *soil* is the K factor raster, and *c_facs* is the raster representing both the C Factor and Manning's roughness coefficient. This analysis showed that approximately 5890 acres (2384 ha), or 9 square miles (23 sq km) of the watershed's 1,076,930 total acres (435,818 ha), or 1,683 square

miles (4,358 sq km) were potential sources of excessive sediment yield. This accounts for 0.5% of the acreage of the watershed.

The slope factor excluded much of the Lower Guyandotte sub-basin, and much of the bare earth activity extracted from the Landsat imagery. The suitability model was recalculated without the slope input:

*con (soil <= 0.24 and c_facs == 1, 1).*

When the slope factor was excluded, the potential source area grew to 37,286 acres (15089 ha), or 144 square miles (373 sq km). This area accounted for 3.5% of the total watershed, and included much of the land cover classes that were considered probable sources (Figure 37). A subset of the Lower Guyandotte sub-basin shows areas of high potential in proximity to a known surface mine (Figure 38).

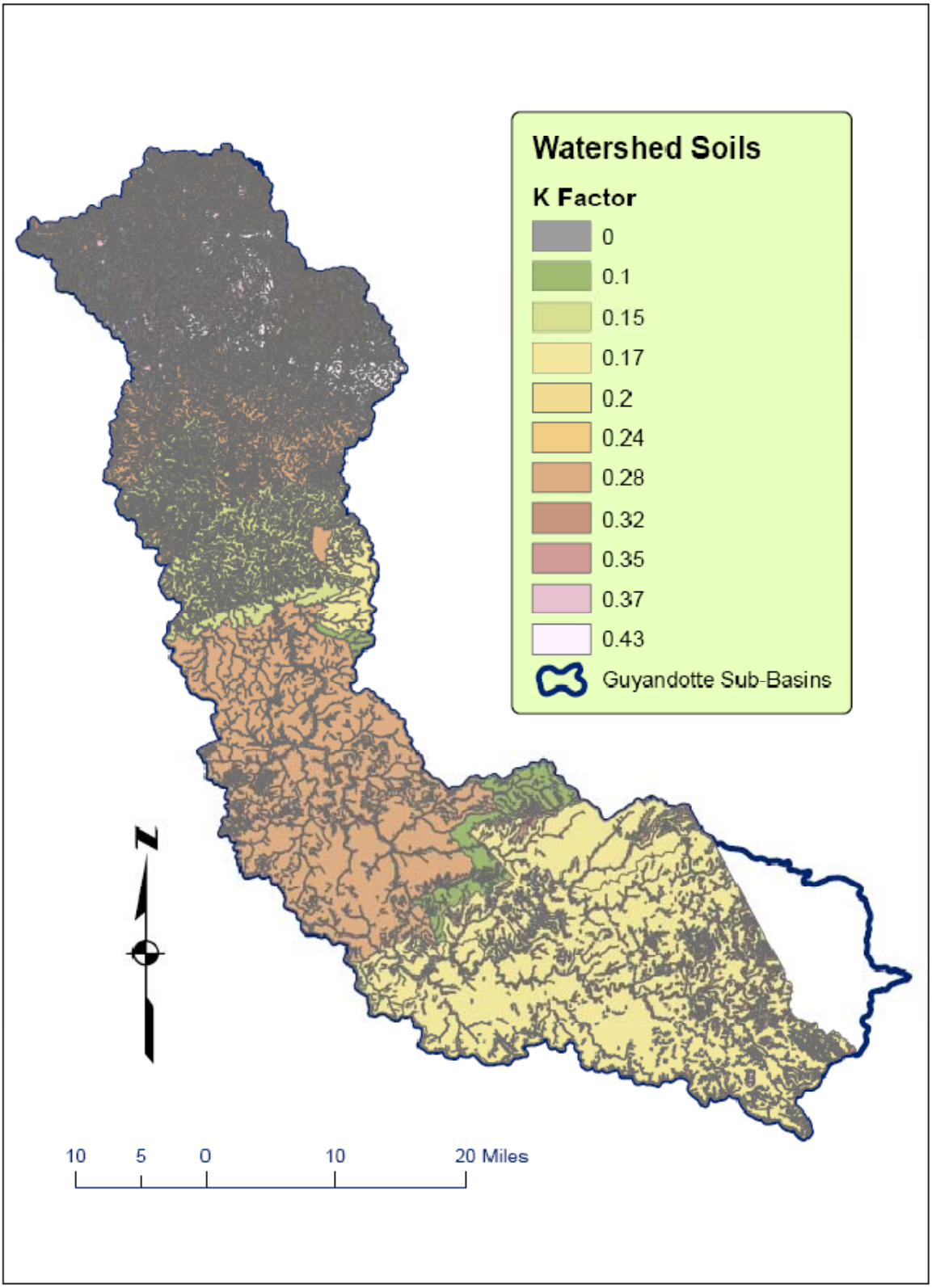


**Figure 34. K Factor, Measuring Soil Erodibility.**

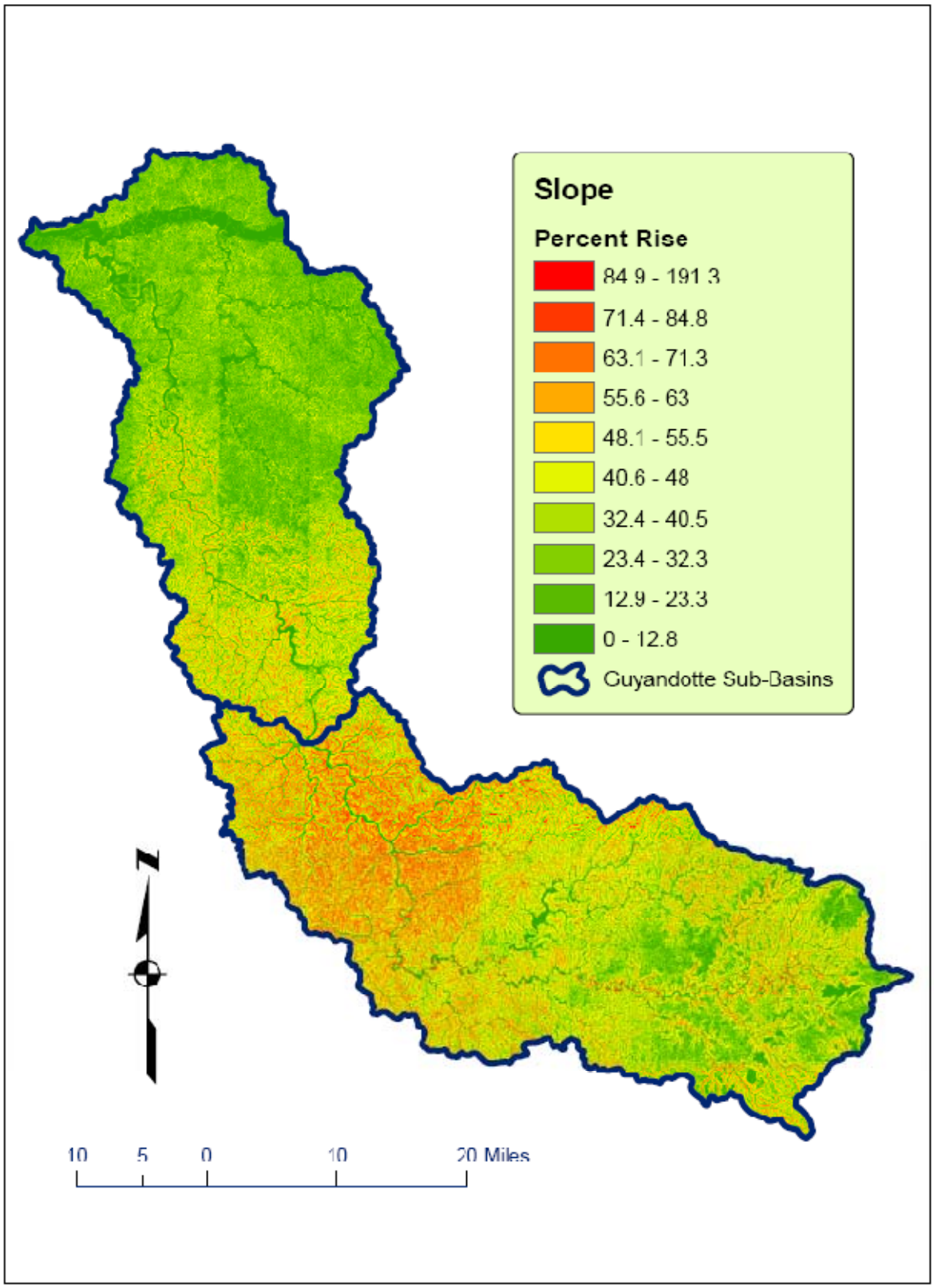


**Figure 35. Slope within Guyandotte Watershed.**

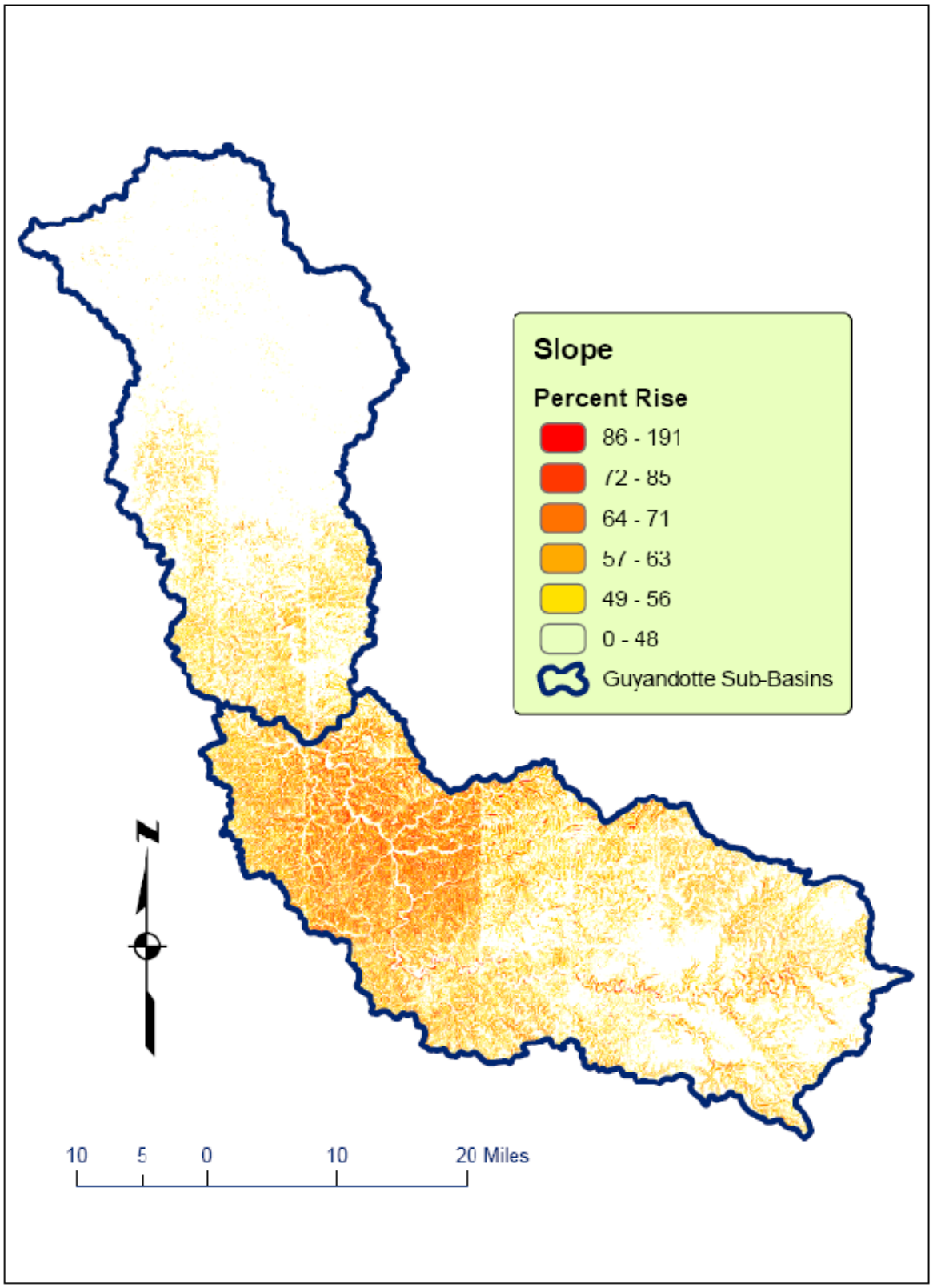


**Figure 36. Slope Greater than 48% within Guyandotte Watershed.**

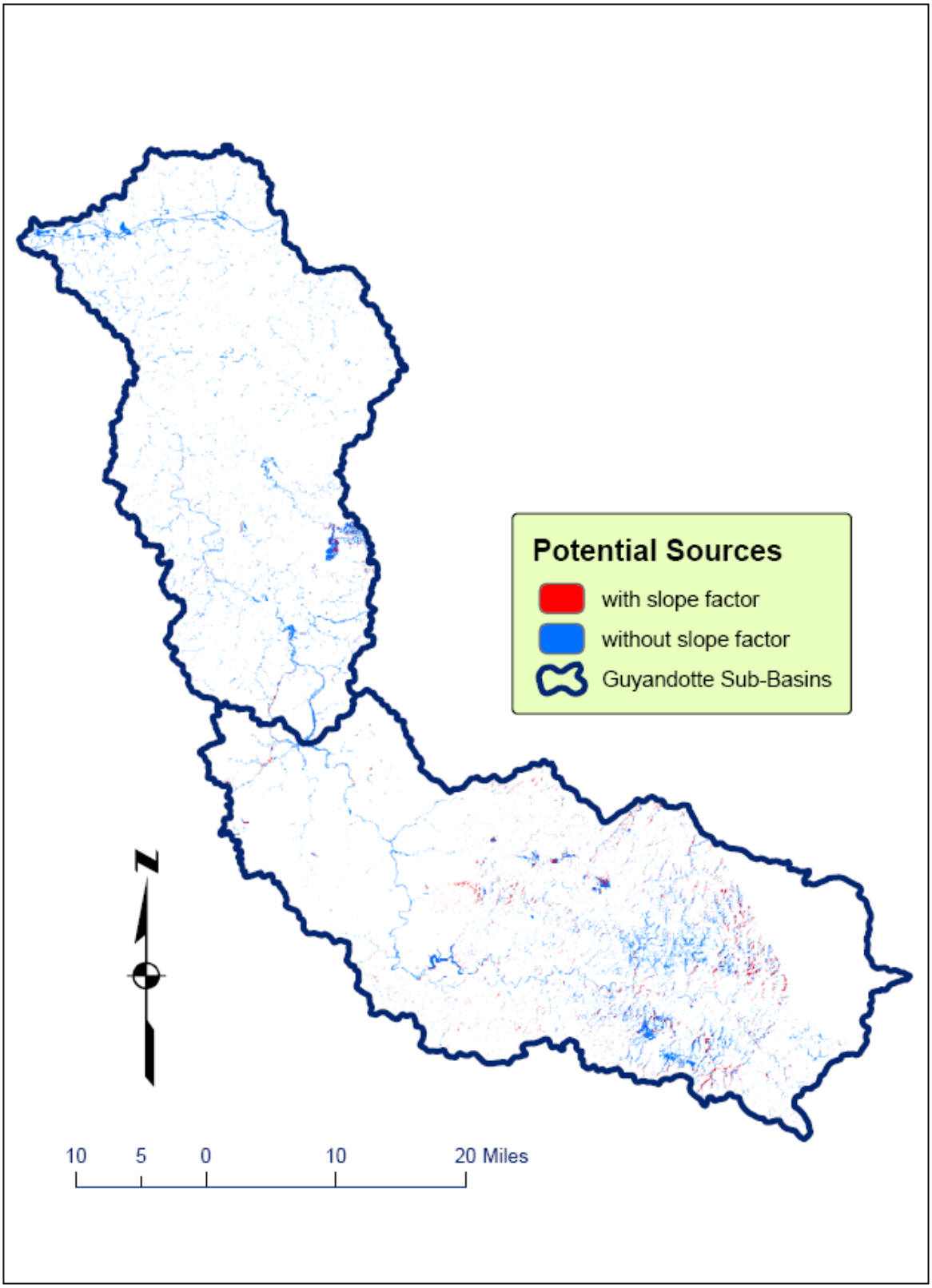


**Figure 37. Comparison of Suitability Models.**

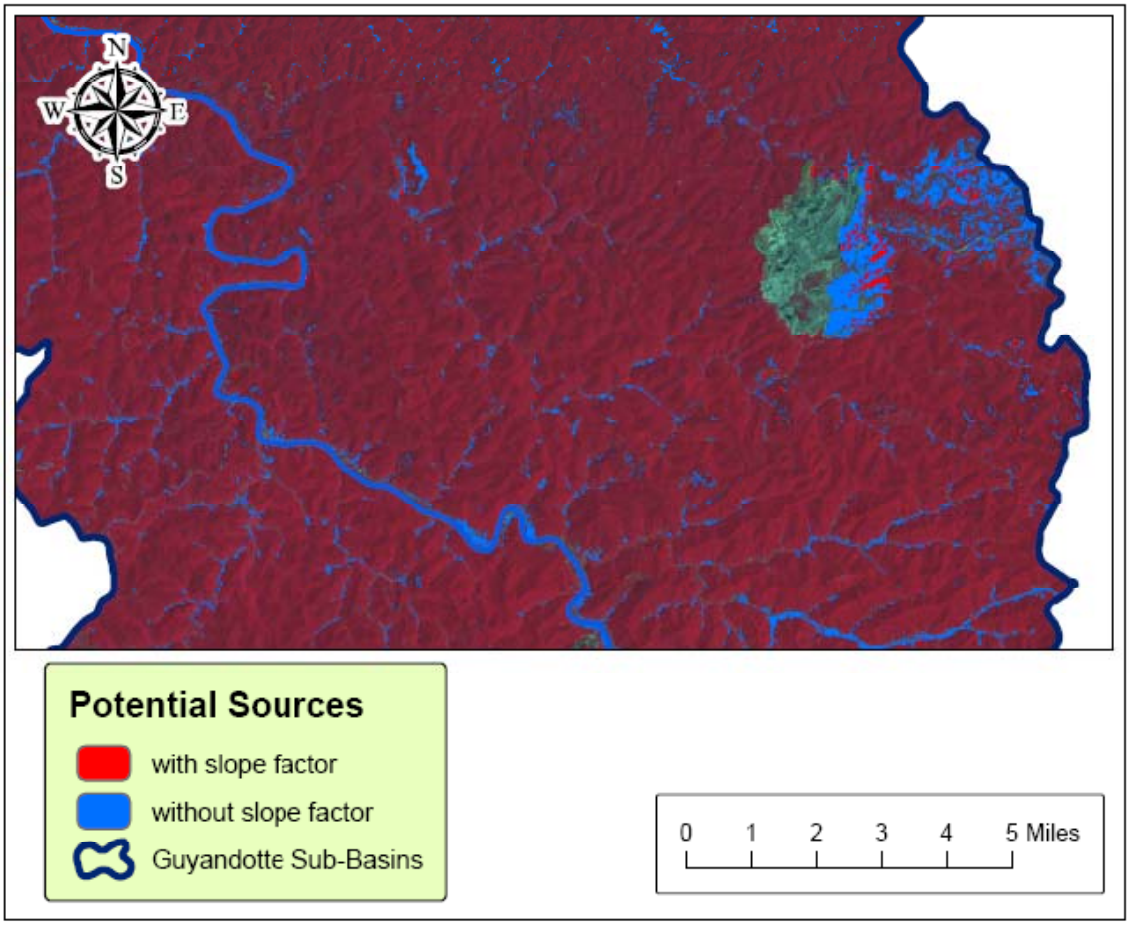


**Figure 38. Subset of Suitability Models over Landsat 7 Color Infrared Image.**

# CHAPTER IV

## Summary

### *Conclusions*

The model successfully showed the potential for remotely sensed imagery to aid in investigations of complex variables where conventional data is lacking. In many sediment yield models, adequate data is available for velocity, bathymetry, discharge, and sediment load. In the area selected for this research, the Greenup Pool of the Ohio River, the data consisted of two points approximately 61.8 river miles apart. The Guyandotte River watershed was used as a test case of the feasibility of this model.

While the sensing of direct parameters of water quality is difficult due to spatial, spectral, and temporal limitations of current sensors, this research shows that relative values can be delivered through indirect means, such as suitability modeling, for a reasonably low cost. The imagery used for this study consisted of two scenes of Landsat 7 ETM+ from May of 2002, and were available free of charge from the USGS. Soil maps and other vector data were available from the West Virginia Geographic Information Systems Technical Center at no cost, as well. Soil Surveys are available at local libraries, online, or from the United States Department of Agriculture Natural Resources Conservation Service. Other sources of tabular data were not free of charge, but their cost was minimal. When compared with the cost of collecting the data from a sufficient number of points to produce a similar data product, it is clear that remote sensing and spatial analysis offers a powerful alternative, or at least, a necessary supporting argument in analysis of water quality.

### *Future Research*

There are detriments to this method, as well. For an example, consider Figure 38, where the model shows potential erosion hazards in proximity to the surface mine. The model did not highlight the mine due to the lack of current information in the soil raster. The soil polygons, from whence came the raster, were generated from soils books that were published as far back as 1975. Even when considering the publication date of the 2007 Lincoln County Soil Survey, the field work would have been completed years prior (Jones 2007). Therefore, there is a clear need to have updated datasets that generally agree temporally for the study area.

The use of Landsat 7 imagery is good for a regional approach, and did produce decent results, however, it would be desirable to use higher resolution imagery, which would produce classifications that would show subtle differences in land cover types. With these subtle differences, the spatial accuracy of models would increase. Although the digital elevation model was not produced by this study, it was produced using Landsat imagery. This was useful for this model due to the 30 m resolution of the classified images, however, higher resolution DEMs are available. Higher resolution of elevation models would mean more accurate stream and runoff calculation, and would make the model more powerful in localized models, such as for individual surface mining permit operations.

Many parameters that should be present in a robust sediment yield model were absent from this model, due mainly to cost of time and resources, but also by limitations of processing power. Parameters for canopy closure,

meteorological data, and underbrush vegetation would increase the modeling power to include raindrop splash erosive force, and increase the efficacy of runoff coefficients.

The methods applied in this research show potential for future, more detailed study of the watershed. The immediate need would be to apply these methods to the remaining watersheds that feed the Greenup Pool, so that comparison data could be assessed. After this is completed, the addition of selected parameters would offer a significant increase in validity of the model.

# CHAPTER V

## Bibliography


Anderson, James R., Ernest E. Hardy, John T. Roach, and Richard E. Witmer.
1976 A *Land Use And Land Cover Classification System For Use With Remote Sensor Data.* Geological Survey Professional Paper 964. A revision of the land use classification system as presented in U.S. Geological Survey Circular 671. United States Government Printing Office, Washington.

Aplin, Paul
2004 *Remote sensing: land cover*. In Progress in Physical Geography 28, 2 (2004) pp. 283–293. Arnold Publishers, London, England.

Aronoff, Stan.
2005 *Remote Sensing for GIS Managers*. ESRI Press. Redlands, CA.

Brewster, H. Steven.
2006 *Bathymetric Data for the Greenup Pool of Ohio River from April to May 2006.* Huntington District, US Army Corps of Engineers.

Bridge, John S.
2003 *Rivers and Floodplains: Forms, Processes, and Sedimentary Record*. Blackwell Publishing. Oxford, UK.

Campbell, James B.
2002 *Introduction to Remote Sensing* (3rd. ed.). The Guilford Press, New York, New York.

Cazenave, A., P.C.D. Milly, H. Douville, J. Benveniste, P. Kosuth, and D. Lettenmaier.
2003 *International Workshop Examines the Role of Space Techniques to Measure Spatio-temporal Change in Terrestrial Waters.* EOS, American Geophysical Union Transactions. Vol. 85, number 6, 2004.

Childs, Colin, Gary Kabot, Makram Murad-al-shaikh.
2004 *Working with ArcGIS Spatial Analyst*. ESRI Press. Redlands, CA:

Cole, Carlos P.
1989 *Soil Survey of Cabell, County, West Virginia*. US Department of Agriculture, Soil Conservation Service.

Cole, Carlos P., Stephen G. Carpenter, and Charles H. Delp.
1985 *Soil Survey of Putnam County, West Virginia.* US Department of Agriculture, Soil Conservation Service.

Cushing, Colbert E. and J. David Allan.
2001 *Streams: Their Ecology and Life.* Academic Press, A Harcourt Science and Technology Company, San Diego, California.

Earth Resource Mapping Pty Ltd.
1999 *ER Mapper 6: Level One Training Workbook for Land Information Applications.* Earth Resource Mapping Pty Ltd. West Perth, Australia.

Easterbrook, Don J.
1969 *Principles of Geomorphology.* McGraw-Hill, Inc., New York.

Eastman, J. Ronald.
2003 *IDRISI Kilimanjaro Guide to GIS and Image Processing*. Clark Labs, Worcester, MA.

Eastman, J. Ronald.
2003 *IDRISI Kilimanjaro Tutorial*. Clark Labs, Worcester, MA.

Ellis, M. M.
1936 *Erosion Silt as a Factor in Aquatic Environments.* Ecology. Vol. 17, No. 1, Ecological Society of America.

Fitzpatrick, F.A., J.C. Knox, and H.E. Whitman.
1999 *Effects of Historical Land-Cover Changes on Flooding and Sedimentation, North Fish Creek, Wisconsin.* USGS Water-Resources Investigations Report 99-4083. U.S. Department of the Interior, U.S. Geological Survey, Reston, VA.

Foster, George R.
2004 *User's Reference Guide: Revised Universal Soil Loss Equation, Version 2 (RUSLE2)* USDA-Agricultural Research Service Washington, D.C.

Franklin, S.E., and M.A. Wulder.
2002 *Remote Sensing Methods in Medium Spatial Resolution Satellite Data Land Cover Classification of Large Areas.* In Progress in Physical Geography 26, 2 (2002) pp.173-205. Arnold Publishers, London, England.

Geladi, Paul, and Hans Grahn.
1996 *Multivariate Image Analysis*. John Wiley & Sons Ltd., Chichester, England.

Gorman, John L. and Lester E. Espy.
1975 *Soil Survey of Fayette and Raleigh Counties, West Virginia.* US Department of Agriculture, Soil Conservation Service.

Gorte, B.G.H.
2000 *Land Use and Catchment Characteristics.* In Gert. A., Shultz and Edwing T. Engman (Eds.), Remote Sensing in Hydrology and Water Management. Springer-Verlag, Berlin Heidelberg. New York, New York.

Haeni, F.P., Marc L. Buursink, John E. Costa, Nick B. Melcher, Ralph T. Cheng, and William J. Plant.
2000 *Ground-Penetrating RADAR Methods Used in Surface-Water Discharge Measurements.* In Noon, David A., Stickley, Glen F., and Longstaff, Dennis, ed., GPR 2000 - Proceedings of the Eighth International Conference on Ground Penetrating Radar: University of Queensland, Queensland, Australia, p.494-500.

Homer, Collin, Jon Dewitz, Joyce Fry, Michael Coan, Nazmul Hossain, Charles Larson, Nate Herold, Alexa McKerrow, J. Nick VanDriel, and James Wickham
2007 *Completion of the 2001 National Land Cover Database for the Conterminous United States*. Photogrammetric Engineering & Remote Sensing Vol. 73, No. 4, April 2007, pp. 337-341. American Society for Photogrammetry & Remote Sensing.

Homer, Collin, Chengquan Huang, Limin Yang, Bruce Wylie, and Michael Coan.
2004 *Development of a 2001 National Land-Cover Database for the United States*. Photogrammetric Engineering & Remote Sensing Vol. 70, No. 7, July 2004, pp. 829–840. American Society for Photogrammetry and Remote Sensing.

Inglis-Smith, Chandra.
2006 *Satellite Image Based Classification Mapping For Spatially Analyzing West Virginia Corridor H Urban Development*. Masters Thesis at Marshall University. Electronic Document. **http://www.marshall.edu/etd/masters/inglis-smith-chandra-2006-ma.pdf** accessed November 20, 2007.

Institute for Water Resources, US Army Corps of Engineers
2004 Waterborne *Commerce of the United States. Calendar Year 2004: Part 2 Waterways and Harbors Gulf Coast, Mississippi River System and Antilles.* Publication IWR-WCUS-04-02. US Army Corps of Engineers. Alexandria, Virginia.

Jain, Manoj K., Umesh C. Kothyari, and Kittur G. Ranga Raju.
2004 *GIS Based Distributed Model for Soil Erosion and Rate of Sediment Outflow from Catchments.* Journal of Hydraulic Engineering. Vol. 131, No. 9. American Society of Civil Engineers, Reston, VA.

Jensen, John R.
2000 *Remote Sensing of Environment: An Earth Resource Perspective.* Pearson-Prentice Hall, Upper Saddle Ridge, New Jersey.

2005 *Introductory Digital Image Processing, A Remote Sensing Perspective*. Pearson-Prentice Hall, Upper Saddle Ridge, New Jersey.

Jones, Richard D.
2007 *Soil Survey of Cabell County, West Virginia.* US Department of Agriculture, Soil Conservation Service.

Leopold, L.B., M.G. Wolman, and J.P. Miller.
1964 *Fluvial Processes in Geomorphology.* W. H. Freeman and Company, San Francisco, CA and London.

Library of Congress
2008 *THOMAS: In the Spirit of Thomas Jefferson, Legislative Information from the Library of Congress*. **http://www.congress.gov** . Website, accessed March 1, 2008.

Lillesand, Thomas M., and Ralph W. Kiefer.
1994 *Remote Sensing and Image Interpretation*. (3rd ed.). John Wiley & Sons, New York, New York.

Lintz, Joseph Jr., and David S. Simonett (Eds.).
1976 *Remote Sensing of Environment*. Addison-Wesley Publishing Co. Advanced Book Program. Reading, Massachusetts.

Lo, C. P.
1986 *Applied Remote Sensing*. Longman Scientific & Technical, Longman Group, UK Ltd. New York, New York.

Mather, A.S.
1986 *Land Use.* Longman, Inc. New York.

McCuen, Richard H.
2005 *Hydrologic Analysis and Design (3rd ed.)*. Pearson Education, Inc. Upper Saddle River, New Jersey.

Meijerink, A.M.J. and C.M.M. Mannaerts.
2000 *Introduction to and General Aspects of Water Management with the aid of Remote Sensing.* In Gert. A., Shultz and Edwing T. Engman (Eds.), Remote Sensing in Hydrology and Water Management. Springer-Verlag, Berlin Heidelberg. New York, New York.

Mitasova, H. and W. M. Brown, M. Hohmann, and S. Warren.
n.d. *Using Soil Erosion Modeling for Improved Conservation Planning: A GIS-based Tutorial.* U.S. Army Corps of Engineers Engineering Research and Development Center. Website **http://skagit.meas.ncsu.edu/~helena/gmslab/reports/CerlErosionTutorial/denix/TutorialAcknowledgements.htm** accessed on December 15th, 2007.

National Aeronautics and Space Administration, Goddard Earth Sciences Data and Information Services Center.
2008 *The Blue, the Bluer, and the Bluest Ocean*. NASA. Webpage **http://disc.sci.gsfc.nasa.gov/**. Accessed August 3, 2008.

Nichols, Gary.
1999 *Sedimentology & Stratigraphy*. Blackwell Science, Ltd. Oxford, England.

Ohio River Board of Engineers.
1929 *Ohio River: Pittsburgh, PA., to Mouth in 280 Charts and Index Sheet.* Ohio River Board of Engineers on Locks and Dams. Louisville, Kentucky.

Ohio River Division, U. S. Army Corps of Engineers.
1979 *Ohio River Navigation: Past - Present – Future.* Ohio River Division of the U. S. Army Corps of Engineers, Cincinnati, Ohio.

1994 *Commerce on the Ohio River and its Tributaries*. 1994 Ohio River Navigation System Report. Ohio River Division of the U. S. Army Corps of Engineers, Huntington, West Virginia.

2003 Ohio *River Navigation Charts: Foster Kentucky to New Martinsville, West Virginia.* U. S. Army Corps of Engineers, Huntington, West Virginia.

Orr, Michael L.
2005 *Phase I Archaeological Survey for the Proposed Northwest Reserve Area, Jefferson District, Lincoln County, West Virginia.* Cultural Resource Analysts, Inc. Contract Publication Series WV05-35. Submitted to Michael Baker, Jr., Inc. Copies available from Cultural Resource Analysts, Inc., Hurricane, West Virginia.

Parker, John T. C.
2000 A Field Guide for the Assessment of Erosion, Sediment Transport, and Deposition in Incised Channels of the Southwestern United States. Water Resources Investigations Report 99-4227. U.S. Department of the Interior, U.S. Geological Survey. Tucson, Arizona.

Price, Maribeth.
2006 *Mastering ArcGIS* (2nd ed.). Boston, MA: McGraw Hill.

Purkis, S.J.
2004 *Calibration of Satellite Images of Reef Environments*. Doctoral dissertation. Vrije Universiteit, Amsterdam, the Netherlands

Purkis, S.J., J.A.M. Kenter, E.K. Oikonomou, and I.S. Robinson.
2002 High-resolution ground verification, cluster analysis and optical model of reef substrate coverage on Landsat TM imagery (Red Sea, Egypt). International Journal of Remote Sensing 23:1677-1698. Electronic Document **http://www.nova.edu/~purkis/publications.htm**. Accessed April 1, 2008.

Rees, W. G.
1990 *Physical Principles of Remote Sensing*. Topics in Remote Sensing 1. Cambridge University Press. Cambridge, England.

Renard, K.G., G.R. Foster, G.A. Weesies, D.K. McCool, and D.C. Yoder.
1997 *Predicting Soil Erosion by Water: A Guide to Conservation Planning with the Revised Universal Soil Loss Equation (RUSLE).* USDA Agriculture Handbook Number 703. United States Department of Agriculture, Washington, D.C.

Rhodes, Rick.
2007 *The Ohio River in American History and Voyaging on Today's River, Along with the Allegheny, Monongahela, Kanawha, Muskingum, Kentucky, Green and Wabash Rivers.* Heron Island Guides. St. Petersburg, FL.

Rott, Helmut.
2000 *Physical Principles and Technical Aspects of Remote Sensing.* In Gert. A., Shultz and Edwing T. Engman (Eds.), Remote Sensing in Hydrology and Water Management. Springer-Verlag, Berlin Heidelberg. New York, New York.

Sabins, Floyd F.
2007 *Remote Sensing, Principles and Interpretation*. W.H. Freeman and Company. New York, New York.

Scheyer, J.M., and K.W. Hipple.
2005. *Urban Soil Primer*. United States Department of Agriculture, Natural Resources Conservation Service, National Soil Survey Center, Lincoln, Nebraska.

Schultz, Gert. A., and Edwing T. Engman (Eds.).
2000 Remote Sensing in Hydrology and Water Management. Springer-Verlag Berlin Heidelberg. New York, New York.

Soil Survey Division Staff.
1993 *Soil survey manual*. USDA NRCS Soil Conservation Service. U.S. Department of Agriculture Handbook 18.

Thanapura, Pravara, Dennis L. Helder, Suzette Burckhard, Eric Warmath, Mary O'Neill, and Dwight Galster.
2007 *Mapping Urban Land Cover Using QuickBird NDVI and GIS Spatial Modeling for Runoff Coefficient Determination*. Photogrammetric Engineering and Remote Sensing. Vol. 73, No. 1, 2007.

The Center for Earth Observation, Yale University
2006 *Creating a Multi-Band or Mosaic Image in ERMapper.* **http://www.yale.edu/ceo** . Website, accessed March 5, 2008.

Tomlin, C. Dana.
1990 *Geographic Information Systems and Cartographic Modeling*. Prentice-Hall, Inc. Englewood Cliffs, New Jersey.

US Army Corps of Engineers
2006 *Ohio River Main Stem System Investment Plan/Programmatic Environmental Impact Statement: Illinois, Indiana, Kentucky, Ohio, Pennsylvania, and West Virginia.* Department of the Army, US Army Engineer District. Lousiville, KY.

USDA NRCS Soil Quality Institute.
2000 *Soil Quality – Urban Technical Note No. 1: Erosion and Sedimentation on Construction Sites*. USDA NRCS Soil Quality Institute. Auburn, AL.

U.S. Geological Survey.
2008 *Earth Explorer.* **http://edcsns17.cr.usgs.gov** . Website, accessed February 27, 2008.

Van Houten, David G., Francis D. Childs, Charles C. Teets, Ronald Estepp, and Frank A. Doonan.
1981 *Soil Survey of Kanawha County, West Virginia.* US Department of Agriculture, Soil Conservation Service.

Verbyla, David L.
1995 *Satellite Remote Sensing of Natural Resources*. Lewis Publishers-CRC Press. Boca Raton, Florida.

Vogelmann, J.E., T.L. Sohl, P.V. Campbell, And D.M. Shaw.
1998 *Regional Land Cover Characterization Using Landsat Thematic Mapper Data and Ancillary Data Sources.* Environmental Monitoring And Assessment 51: 415–428, 1998. Kluwer Academic Publishers, Netherlands.

West Virginia GIS Technical Center.
2007 *West Virginia GIS Technical Center*. **http://wvgis.wvu.edu/**. Website. Frequent access.

Wikipedia.org
2008 *Electromagnetic Spectrum*. **http://en.wikipedia.org** Website, accessed July 3, 2008.

Wilkie, David S. and John T. Finn.
1996 *Remote Sensing Imagery for Natural Resources Monitoring: A Guide for First Time Users.* Columbia University Press. New York.

Wolf, Barrie L.
1988 *Soil Survey of Wyoming County, West Virginia.* US Department of Agriculture, Soil Conservation Service.

1994 *Soil Survey of Boone County, West Virginia.* US Department of Agriculture, Soil Conservation Service.

# Appendix A

## Natural Resources Conservation Service Soils within Guyandotte Watershed with Erodibility Factor

The following table contains Natural Resources Conservation Service (NRCS) soil symbols that were located within the Guyandotte Watershed. The K Factor was added from tabular data in the soil surveys of Boone, Cabell, Kanawha, Lincoln, Putnam, and Wyoming counties (Cole 1989; Cole et al. 1985; Jones 2007; Van Houten et al. 1981; Wolf 1988 and 1994). No soil shapefile was available for Raleigh County, so it was omitted from analysis and this appendix. Logan and Mingo counties did not have a published soil survey available, so K Factors for those soils were added from adjacent surveys where possible. A K Factor of 0 had to be accepted for several soil types due to lack of data. Names and descriptions of these soils can be obtained from the soil surveys of the aforementioned counties.

| *NRCS Symbol* | *MUKEY* | *K Factor* |
|---|---|---|
| AbB | 1155533 | 0.32 |
| AgA | 513150 | 0.32 |
| AgB | 553311 | 0.32 |
| AgC | 513152 | 0.32 |
| AhC | 513637 | 0.32 |
| BeD | 553364 | 0.32 |
| BeE | 553379 | 0.32 |
| BPF | 513488 | 0.17 |
| BrG | 1155534 | 0.28 |
| BSF | 1155535 | 0.17 |
| Ca | 513640 | 0.32 |
| CDF | 512830 | 0.24 |
| CeB | 532203 | 0.32 |
| CeF | 513489 | 0.32 |
| Cg | 513490 | 0.32 |
| CgF | 514853 | 0.37 |
| Ch | 1155536 | 0.37 |
| Ck | 1155537 | 0.32 |
| CoA | 553361 | 0.37 |
| CoB | 513155 | 0.43 |
| CoC | 513156 | 0.43 |
| Cr | 1155538 | 0.32 |
| CrF | 532204 | 0.32 |
| CtB | 513644 | 0.37 |
| Cu | 513492 | 0.32 |
| CuB | 553359 | 0.43 |
| CuC | 553358 | 0.43 |
| DgF | 515008 | 0.37 |
| DlD | 553340 | 0.43 |
| DlE | 515009 | 0.43 |

| *NRCS Symbol* | *MUKEY* | *K Factor* |
|---|---|---|
| DoD | 513645 | 0.43 |
| DPF | 513493 | 0.17 |
| DrD | 515010 | 0.24 |
| DrE | 515011 | 0.24 |
| FkC | 1155539 | 0.28 |
| FkF | 1155540 | 0.28 |
| FvE | 513494 | 0.32 |
| GiD | 553349 | 0.32 |
| GiE | 559311 | 0.32 |
| GlC | 513157 | 0.32 |
| GlD | 513647 | 0.32 |
| GlE | 532208 | 0.32 |
| GlF | 553350 | 0.37 |
| GmE | 1155542 | 0.24 |
| GpC | 513495 | 0.32 |
| GpD | 553318 | 0.32 |
| GpE | 513496 | 0.37 |
| GpF | 553320 | 0.43 |
| GrE | 553351 | 0.32 |
| GRF | 512839 | 0.32 |
| Gs | 553337 | 0.20 |
| GsC3 | 512845 | 0.32 |
| GsD3 | 512846 | 0.32 |
| Gt | 1412599 | 0.20 |
| Gu | 553355 | 0.32 |
| GuC | 515013 | 0.32 |
| GuC3 | 513159 | 0.32 |
| GuD | 515014 | 0.32 |
| GuD3 | 513161 | 0.32 |
| GuE | 515015 | 0.32 |

| *NRCS Symbol* | *MUKEY* | *K Factor* |
|---|---|---|
| GuE3 | 513163 | 0.32 |
| GuF | 515016 | 0.32 |
| GuF3 | 513165 | 0.32 |
| GvE | 513166 | 0.17 |
| GvF | 513167 | 0.17 |
| Gw | 1155543 | 0.32 |
| GwE | 514857 | 0.32 |
| GxD | 513657 | 0.35 |
| Gy | 513658 | 0.37 |
| Gz | 513659 | 0.37 |
| HaA | 513168 | 0.32 |
| HaB | 513169 | 0.32 |
| HgE | 1155544 | 0.32 |
| HMF | 1155545 | 0.15 |
| Ho | 513497 | 0.28 |
| HuE | 1155546 | 0.15 |
| Hy | 553367 | 0.28 |
| ImE | 513498 | 0.32 |
| ImF | 1155547 | 0.32 |
| ItF | 513499 | 0.32 |
| KaA | 513171 | 0.32 |
| KaB | 532216 | 0.32 |
| KcF | 1155550 | 0.32 |
| KeB | 514862 | 0.32 |
| KfB | 1155548 | 0.28 |
| KfF | 1155549 | 0.28 |
| KmF | 513501 | 0.32 |
| KnA | 513663 | 0.32 |
| KnB | 513664 | 0.32 |
| KrF | 532220 | 0.32 |

| *NRCS Symbol* | *MUKEY* | *K Factor* |
|---|---|---|
| KuB | 513665 | 0.32 |
| LdE | 514865 | 0.28 |
| LgC | 515022 | 0.43 |
| LgD | 515023 | 0.43 |
| LiD | 553323 | 0.28 |
| LiE | 559309 | 0.28 |
| LlC | 532223 | 0.28 |
| LlD | 513174 | 0.28 |
| LlE | 513175 | 0.28 |
| LmE | 1155552 | 0.32 |
| Lo | 553370 | 0.37 |
| MaB | 513671 | 0.43 |
| MaC | 513672 | 0.43 |
| MgB | 513502 | 0.43 |
| MgC | 513180 | 0.43 |
| MHF | 1155553 | 0.28 |
| MlE | 553345 | 0.15 |
| Mo | 513181 | 0.32 |
| MoB | 513674 | 0.43 |
| MoC | 513675 | 0.43 |
| MPF | 1155555 | 0.10 |
| Mr | 553366 | 0.32 |
| Ms | 553327 | 0.37 |
| MuC | 513676 | 0.43 |
| Ne | 553354 | 0.37 |
| Or | 553371 | 0.37 |
| PbC | 513503 | 0.20 |
| PbE | 515032 | 0.28 |
| PBF | 1155556 | 0.17 |
| PcE | 513504 | 0.20 |
| PlE | 532232 | 0.15 |
| PnE | 1155557 | 0.20 |
| Po | 513677 | 0.24 |
| PoB | 513505 | 0.24 |
| PuB | 513506 | 0.24 |
| PvE | 553378 | 0.20 |
| RmF | 557377 | 0.28 |
| SbB | 1155559 | 0.24 |
| Sc | 553328 | 0.32 |
| Se | 513182 | 0.32 |

| *NRCS Symbol* | *MUKEY* | *K Factor* |
|---|---|---|
| SeA | 553329 | 0.24 |
| SeB | 1155560 | 0.24 |
| SeC | 513507 | 0.32 |
| Sf | 513183 | 0.32 |
| SfB | 553330 | 0.24 |
| ShF | 553342 | 0.24 |
| SkC | 553381 | 0.28 |
| SlD | 553376 | 0.28 |
| SlE | 532152 | 0.28 |
| Sm | 553341 | 0.24 |
| Sn | 513184 | 0.20 |
| SoA | 513678 | 0.24 |
| SrB | 513185 | 0.20 |
| SvC | 513680 | 0.24 |
| SwF | 514869 | 0.32 |
| TlB | 513186 | 0.43 |
| Ty | 513187 | 0.43 |
| Ua | 1155561 | 0.00 |
| UA | 513188 | 0.00 |
| Ub | 1155562 | 0.00 |
| UcB | 1155570 | 0.00 |
| Ud | 513508 | 0.00 |
| UeC | 513193 | 0.37 |
| Uf | 1155564 | 0.00 |
| UgC | 513195 | 0.37 |
| UgD | 513197 | 0.37 |
| UgE | 513199 | 0.37 |
| UkB | 1155566 | 0.32 |
| UnB | 1155567 | 0.32 |
| UoB | 513204 | 0.43 |
| UpC | 513682 | 0.37 |
| Ur | 513683 | 0.00 |
| Us | 513684 | 0.32 |
| UtB | 1155568 | 0.00 |
| UuB | 553380 | 0.00 |
| UvC | 513205 | 0.43 |
| Uw | 1408560 | 0.00 |
| VaB | 512871 | 0.37 |
| VaC | 513206 | 0.37 |
| VaD | 513207 | 0.37 |

| *NRCS Symbol* | *MUKEY* | *K Factor* |
|---|---|---|
| VaE | 513208 | 0.37 |
| VbD | 513209 | 0.32 |
| VdD3 | 513210 | 0.37 |
| VeB | 513211 | 0.43 |
| VeC | 513212 | 0.43 |
| VnD | 553335 | 0.37 |
| VnE | 553336 | 0.37 |
| VuD | 513687 | 0.37 |
| W | 1155573 | 0.00 |
| Ye | 1155572 | 0.24 |
| Yg | 553348 | 0.17 |